

Efficient megakaryopoiesis and platelet production require phospholipid remodeling and PUFA uptake through CD36

Barrachina, Maria N.; Pernes, Gerard; Becker, Isabelle C.; Allaey, Isabelle; Hirsch, Thomas I.; Groeneveld, Dafna J.; Khan, Abdullah O.; Freire, Daniela; Guo, Karen; Carminita, Estelle; Morgan, Pooranee K.; Collins, Thomas J. C.; Mellett, Natalie A.; Wei, Zimu; Almazni, Ibrahim; Italiano, Joseph E.; Luyendyk, James; Meikle, Peter J.; Puder, Mark; Morgan, Neil V.

DOI:

[10.1038/s44161-023-00305-y](https://doi.org/10.1038/s44161-023-00305-y)

License:

Other (please specify with Rights Statement)

Document Version

Peer reviewed version

Citation for published version (Harvard):

Barrachina, MN, Pernes, G, Becker, IC, Allaey, I, Hirsch, TI, Groeneveld, DJ, Khan, AO, Freire, D, Guo, K, Carminita, E, Morgan, PK, Collins, TJC, Mellett, NA, Wei, Z, Almazni, I, Italiano, JE, Luyendyk, J, Meikle, PJ, Puder, M, Morgan, NV, Boilard, E, Murphy, AJ & Machlus, KR 2023, 'Efficient megakaryopoiesis and platelet production require phospholipid remodeling and PUFA uptake through CD36', *Nature Cardiovascular Research*, vol. 2, no. 8, pp. 746-763. <https://doi.org/10.1038/s44161-023-00305-y>

[Link to publication on Research at Birmingham portal](#)

Publisher Rights Statement:

This version of the article has been accepted for publication, after peer review (when applicable) and is subject to Springer Nature's AM terms of use, but is not the Version of Record and does not reflect post-acceptance improvements, or any corrections. The Version of Record is available online at: <https://doi.org/10.1038/s44161-023-00305-y>

General rights

Unless a licence is specified above, all rights (including copyright and moral rights) in this document are retained by the authors and/or the copyright holders. The express permission of the copyright holder must be obtained for any use of this material other than for purposes permitted by law.

- Users may freely distribute the URL that is used to identify this publication.
- Users may download and/or print one copy of the publication from the University of Birmingham research portal for the purpose of private study or non-commercial research.
- User may use extracts from the document in line with the concept of 'fair dealing' under the Copyright, Designs and Patents Act 1988 (?)
- Users may not further distribute the material nor use it for the purposes of commercial gain.

Where a licence is displayed above, please note the terms and conditions of the licence govern your use of this document.

When citing, please reference the published version.

Take down policy

While the University of Birmingham exercises care and attention in making items available there are rare occasions when an item has been uploaded in error or has been deemed to be commercially or otherwise sensitive.

If you believe that this is the case for this document, please contact UBIRA@lists.bham.ac.uk providing details and we will remove access to the work immediately and investigate.

1 **Efficient megakaryopoiesis and platelet production require phospholipid remodeling and**
2 **PUFA uptake through CD36**

3
4 Maria N Barrachina^{1,2}, Gerard Pernes³, Isabelle C Becker^{1,2}, Isabelle Allaey⁴, Thomas I. Hirsch^{1,2},
5 Dafna J Groeneveld⁵, Abdullah O. Khan^{6,7}, Daniela Freire¹, Karen Guo¹, Estelle Carminita^{1,2},
6 Pooranee K Morgan³, Thomas J. C. Collins³, Natalie A Mellett⁸, Zimu Wei⁵, Ibrahim Almazni⁶,
7 Joseph E. Italiano^{1,2}, James Luyendyk⁵, Peter J Meikle⁸, Mark Puder^{1,2}, Neil V. Morgan⁶, Eric
8 Boilard⁴, Andrew J Murphy³, Kellie R Machlus*^{1,2}

9
10 ¹ Vascular Biology Program, Boston Children's Hospital, Boston, MA, 02115 USA

11 ² Harvard Medical School, Department of Surgery, Boston Children's Hospital, Boston, MA,
12 02115 USA

13 ³ Haematopoiesis and Leukocyte Biology, Baker Heart and Diabetes Institute, Melbourne, VIC,
14 Australia

15 ⁴ Centre de Recherche du CHU de Québec-Université Laval and Centre de Recherche
16 ARThrite, Québec, QC, G1V4G2 Canada

17 ⁵ Department of Pathobiology and Diagnostic Investigation, Michigan State University, East
18 Lansing, MI, USA

19 ⁶ Institute of Cardiovascular Sciences, College of Medical and Dental Sciences, University of
20 Birmingham, Vincent Drive, Birmingham, U.K, B15 2TT

21 ⁷ MRC Weatherall Institute of Molecular Medicine, Radcliffe Department of Medicine and
22 National Institute of Health Research (NIHR) Oxford Biomedical Research Centre, University
23 of Oxford, Oxford, U.K. OX3 9DS

24 ⁸ Metabolomics, Baker Heart and Diabetes Institute, Melbourne, VIC, Australia

25
26
27
28
29
30
31
32
33 ***Correspondence to:**

34 Kellie R Machlus

35 1 Blackfan Circle, Karp 11.214

36 Boston, MA 02115

37 Kellie.Machlus@childrens.harvard.edu

38
39 Word Count: 4755

40 Figures: 7

41 Tables: 1

42 Extended Data Figures: 7

43 Extended Data Tables: 2

44 Supplementary Tables: 2

45
46
47
48
49
50
51
52
53
54
55
56
57
58
59
60
61
62
63
64
65
66
67
68
69
70
71
72
73
74
75
76
77
78
79

ABSTRACT

Lipids contribute to hematopoiesis and membrane properties and dynamics; however, little is known about the role of lipids in megakaryopoiesis. Here we show that megakaryocyte progenitors, megakaryocytes, and platelets present a unique lipidome progressively enriched in polyunsaturated fatty acid (PUFA)-containing phospholipids. In vitro, inhibition of both exogenous fatty acid functionalization and uptake, and de novo lipogenesis impaired megakaryocyte differentiation and proplatelet production. In vivo, mice on a high saturated fatty acid diet had significantly lower platelet counts, which was prevented by eating a PUFA-enriched diet. Fatty acid uptake was largely dependent on CD36, and its deletion in mice resulted in low platelets. Moreover, patients with a *CD36* loss-of-function mutation exhibited thrombocytopenia and increased bleeding. Our results suggest that fatty acid uptake and regulation is essential for megakaryocyte maturation and platelet production, and that changes in dietary fatty acids may be a viable target to modulate platelet counts.

EDITOR'S SUMMARY

Barrachina et al. present an extensive lipidomic analysis at different stages of thrombopoiesis and, through in vitro and in vivo experiments, demonstrate that fatty acid uptake, largely dependent on the scavenger receptor CD36, and its regulation are essential for megakaryocyte maturation and platelet production.

80 Lipids are key for many cell biological processes including membrane construction, organelle
81 compartmentalization, energy storage, and the assembly of signaling effectors.¹ In addition,
82 recent studies have demonstrated a role for lipids in cell fate decisions during hematopoiesis.²⁻⁵
83 Cells obtain lipids in several ways; essential fatty acids are taken up from the diet (mostly
84 polyunsaturated fatty acids, PUFAs, containing multiple double bonds), while saturated fatty acids
85 (SFAs, no double bonds) can be produced via *de novo* lipogenesis.⁶ As such, how lipids are
86 produced and incorporated into cells can be regulated through cellular metabolism and dietary
87 intervention.⁵ Megakaryocytes (MKs) are large hematopoietic cells that primarily reside in the
88 bone marrow and produce platelets, which are essential for hemostasis.^{7,8} Even though MKs have
89 an extensive, lipid-rich membrane system, the role of lipids in their maturation and during platelet
90 production has not been extensively investigated.

91 Megakaryopoiesis is the process by which MKs develop from hematopoietic stem cells (HSCs)
92 along the myeloid branch of hematopoiesis under the direction of thrombopoietin (TPO) signaling
93 through its receptor myeloproliferative leukemia virus (MPL). According to the classical model,
94 each mature MK is derived from an HSC that sequentially transitions through the multipotent
95 progenitor (MPP), common myeloid progenitor (CMP), MK-erythroid progenitor (MEP), and MK
96 progenitor (MKP) state.⁹ After MKs are terminally differentiated, they undergo maturation^{7,8} which
97 includes increasing in size and developing an extensive demarcation membrane system (DMS).
98 The DMS is a highly intertwined membrane network with numerous side branches and multiple
99 connections with the cell surface which serves as the membrane reservoir for proplatelet
100 formation and ultimately becomes the plasma membrane of platelets.^{8,10} MKs then extend long
101 proplatelet extensions through endothelial cells and into the vessel lumen and bloodstream,
102 where they rapidly undergo repeated rounds of fission, becoming 1-3 μm circulating platelets.^{7,8}
103 The identification of modulators of MK maturation and platelet production is essential, as
104 thrombocytopenia (platelet counts $< 150 \times 10^9/\text{L}$) can be life-threatening due to a heightened risk
105 of bleeding.^{11,12} Current standard of care is limited to therapeutics such as TPO receptor agonists
106 which can have severe side effects including bone marrow fibrosis and leukemic transformation.¹³⁻
107 ¹⁵ Therefore, there is an urgent need to identify new thrombopoietic agents to increase platelet
108 counts.

109 Due to the extensive DMS unique to MKs, we postulated that MKs may be more reliant on a
110 particular membrane lipid composition than other cell types. Specifically, the processes of DMS
111 formation and proplatelet production require a profound reorganization of both the MK
112 cytoskeleton and the accompanying membrane system as the DMS folds and then extrudes itself
113 outward and subsequently thins into proplatelet shafts.^{7,8} To accomplish this, the MK membrane
114 must acquire the lipids necessary over the course of its maturation to have sufficient flexibility for
115 these processes. Critically, the higher number of double bonds in PUFAs significantly enhance
116 membrane fluidity.¹⁶

117 While the function of lipids in platelet production remains ambiguous, recent work has begun to
118 suggest a role for lipids in MK maturation. Valet et al.¹⁷ showed that MKs can take up fatty acids
119 released by adipocytes via CD36 to facilitate their maturation *in vitro*. In addition, Kelly et al.
120 demonstrated that the *de novo* lipogenesis pathway can regulate late-stage MK maturation and
121 platelet formation.¹⁸ These studies support a role for lipids in MK maturation and raise further
122 questions about the relationship between megakaryopoiesis and lipid biosynthesis. Here, we

123 expand the previously suggested role of lipids in MKs by performing lipidomics to uncover the
124 lipid fingerprint of MEPs, immature and mature MKs, and platelets. We demonstrate that altering
125 both *de novo* lipogenesis and fatty acid functionalization and uptake abrogate megakaryopoiesis
126 and proplatelet formation. Further, we reveal that platelet counts can be modulated *in vivo* by
127 altering dietary fatty acid content. Finally, we identify CD36 as a key fatty acid uptake receptor
128 that affects platelet counts in both mice and humans. These data support a key role for fatty acids
129 in MK maturation and platelet production and suggest that dietary interventions can influence
130 thrombopoiesis.

131

132 **RESULTS**

133 **MKs and platelets display a unique profile enriched in PUFAs**

134 To provide insight into how the cellular lipid profile changes throughout MK differentiation and
135 maturation, we performed a lipidomic study using liquid chromatography tandem-mass
136 spectrometry (LC-MS/MS) starting with MEPs. The indicated cell populations were sorted from
137 adult murine bone marrow and platelets were isolated from autologous blood (Fig. 1a).
138 Dimensionality reduction of all populations revealed that MKs and platelets have a lipidome
139 distinct from their precursor, MEPs (Fig. 1b), which was confirmed when analyzing different lipid
140 class compositions (Extended data Fig. 1a). These data suggest that extensive remodeling of the
141 lipidome occurs during megakaryocyte maturation. Further, when comparing the lipid composition
142 of the microenvironment to the cells that reside in it, such as comparing bone marrow extracellular
143 fluid (BMEF) to bone marrow cells (Extended data Fig. 1b-d) or plasma to platelets (Extended
144 data Fig. 1e), we found that the lipid composition of these cells (Extended data Fig. 1f-i) was
145 unique to their environments. We used a lipid ontology analysis to identify the main lipid species
146 that varied between the different cell populations and found that membrane lipids,
147 glycerophospholipids, and fatty acids were upregulated over the course of megakaryo- and
148 thrombopoiesis (Fig. 1c). This was further supported by analysis of an mRNA sequencing dataset
149 previously published by our group¹⁹ which revealed that MKs are actively regulating key lipid-
150 related mRNAs as they undergo proplatelet formation (Fig. 1d-e), specifically highlighting
151 pathways involved in fatty acid metabolism and uptake. A pathway analysis further emphasized
152 the synthesis of the long chain fatty acyl-CoA and fatty acid metabolism as key pathways involved
153 in proplatelet production (Fig. 1e). Therefore, as lipidomic and mRNA pathway analyses
154 suggested that differences in phospholipids and fatty acids were unique and important to MK
155 maturation and platelet production, we analyzed these lipid classes in our cell populations. Our
156 data revealed that MKs and platelets were enriched in phosphatidylcholine (PC) compared to their
157 progenitors. Conversely, MKs and platelets were reduced in phosphatidylethanolamine (PE),
158 phosphatidylglycerol (PG), and phosphatidylinositol (PI) (Fig. 1f). When examining the differences
159 in the overall fatty acid saturation level, we identified a significant reduction in saturated fatty acids
160 (no double bonds) along the maturation pathway (Fig 1g-h). Notably, we also found that cells
161 acquired increasing levels of more complex PUFA-containing phospholipids (6+ double bonds,
162 Fig. 1g, i) as they matured, with platelets exhibiting the highest levels. This overall pattern of fatty
163 acid remodeling was also seen in other phospholipid classes such as PC, PE, PI, and
164 phosphatidylserine (PS) (Extended data Fig. 1d-g). Taken together, these data reveal significant
165 phospholipid remodeling, and specifically an increase in PUFAs during megakaryopoiesis.

166 **Fatty acids are essential for MK and platelet production**

167 Since we identified that PUFA content increases throughout megakaryopoiesis, we hypothesized
168 that PUFA uptake is important for MK maturation and platelet production. PUFAs are either
169 obtained from the diet and are therefore considered essential fatty acids or are synthesized from
170 essential fatty acid precursors. To test the importance of fatty acid uptake and functionalization in
171 MK differentiation and proplatelet formation, we inhibited ACSL, the enzyme that catalyzes the
172 formation of acyl-CoA from fatty acids, a necessary step for the functionalization of fatty acids and
173 their incorporation into phospholipids (Fig. 2a). We isolated murine bone marrow- (Fig. 2) and
174 fetal liver-derived (Extended data Fig. 2) hematopoietic stem and progenitor cells (HSPCs) and
175 cultured them with TPO for 4 days with the indicated concentrations of the ASCL inhibitor Triacsin
176 C. Inhibition of ACSL led to a significant, dose dependent reduction in the number of immature
177 (CD41⁺) and mature (CD41/42⁺) MKs in both bone marrow- (Fig. 2b-c) and fetal liver (Extended
178 data Fig. 2a)-derived MKs.

179 Next, we inhibited *de novo* lipogenesis using inhibitors of acyl-coA carboxylase (ACC, PF-
180 05175175) and fatty acid synthetase (FASN, Cerulenin) (Fig. 2d). Both inhibitors significantly and
181 dose dependently reduced MK maturation in bone marrow- (Fig. 2e-f) and fetal liver-derived
182 (Extended data Fig. 2 c-d) MKs. Notably, the frequency of mature MKs (CD41/42⁺) was decreased
183 more than immature MKs (CD41⁺). None of the inhibitors were cytotoxic (Extended data Fig. 2b,
184 d, f), suggesting that the effects on HSPCs were due to a failure in MK differentiation and not cell
185 death.

186 Once mature, MKs remodel their DMS into proplatelets. We postulated that this process is
187 dependent on a highly specific membrane lipid content to allow for proplatelet elaboration. To
188 explore the role of fatty acid uptake/functionalization and synthesis on proplatelet formation, we
189 treated mature MKs (day 4 of culture, i.e. 24h preceding proplatelet formation) with the indicated
190 inhibitors and monitored proplatelet formation over 24 hours (Fig. 2g). Triacsin C treatment
191 resulted in a significant reduction in both the number of MKs making proplatelets and the area of
192 formed proplatelets (Fig. 2h-j), suggesting a severe impairment in proplatelet elaboration.
193 However, neither of the *de novo* lipogenesis inhibitors significantly impacted proplatelet formation
194 (Fig. 2k-n), indicating that *de novo* lipogenesis may not be essential for proplatelet generation. To
195 exclude the possibility that effects on proplatelet formation were due to impaired mitochondrial
196 activity, we measured oxygen consumption rate using a Seahorse mitostress assay of murine
197 bone marrow-derived MKs treated with the indicated inhibitors. The MK mitochondrial profile was
198 not altered upon inhibition of fatty acid synthesis with Triacsin C, Cerulenin, or PF-051751
199 (Extended data Fig. 2g-h), supporting our conclusion that the observed changes in MK maturation
200 and/or proplatelet formation were due to a role of fatty acids in membrane incorporation and not
201 mitochondrial metabolism. Together, these data suggest that MK differentiation and maturation
202 are reliant on both fatty acid uptake and *de novo* lipogenesis. However, proplatelet formation
203 appears uniquely reliant on fatty acid uptake and functionalization.

204

205 **SFA-enriched high fat diet reduces platelet counts**

206 Our data demonstrated that megakaryopoiesis and platelet production are dependent on fatty
207 acid uptake, functionalization, and metabolism. We therefore postulated that altering the

208 exogenous supply of fatty acids will alter MK phenotype and subsequent platelet production. We
209 first wanted to examine the effects of direct supplementation of SFAs on MK development and
210 platelet production. To confirm and visualize SFA incorporation into MKs *in vitro*, we performed
211 click-chemistry using palmitic acid modified with a terminal alkyne group. First, HSPCs isolated
212 from murine bone marrow were supplemented with modified SFA in culture. After 4 days, mature
213 MKs were functionalized with an azide-linked fluorescent reporter, which bound modified palmitic
214 acid in the MK membrane (Fig. 3a), allowing its visualization (Fig. 3b). We observed a robust,
215 dose-dependent incorporation of palmitic acid throughout the plasma and demarcation
216 membranes of MKs (Fig. 3b-c). Additionally, MKs supplemented with palmitic acid were
217 significantly larger and displayed a reduced capacity to form proplatelets *in vitro* (Fig. 3d-e). These
218 data confirmed that MKs incorporated SFAs (palmitic acid) into their membrane as they
219 differentiate and mature, resulting in increased size and decreased proplatelet generation.

220 To test the impact of an SFA-enriched diet *in vivo*, male mice were fed a 60% high fat diet (diet-
221 induced obesity (DIO) model) for 14 weeks (Fig. 3f), which led to increased body weight (Fig. 3g).
222 To determine whether this high fat diet affected HSPC differentiation, we quantified the number
223 of bone marrow HSPCs by flow cytometry. While we did not detect differences between long term
224 (LT)-HSC, Pre-GM, or Pre-MK populations after 14 weeks, we found a significant increase in
225 short-term (ST)-HSCs and Pre-MKs (Fig. 3h). Further, bone marrow MKs were significantly larger
226 in DIO mice (Fig. 3i-j), consistent with our *in vitro* data (Fig. 3d), while their numbers were
227 unchanged. Finally, platelet counts were significantly reduced after administration of the SFA-
228 enriched diet (Fig. 3k). No significant differences were found in other blood parameters (Extended
229 data Fig. 3a-e). To confirm that the reduction in platelet counts was not due to differences in
230 platelet clearance, we performed an *in vivo* platelet lifespan assay and found no differences
231 between the DIO and control mice (Extended data Fig. 3f). These data revealed that enriched
232 dietary SFAs increased MK size and decreased platelet production both *in vitro* and *in vivo*.
233 Further, these data support our hypothesis that enhanced membrane PUFA content is necessary
234 for maximal proplatelet production, and that interruption of this process through increased dietary
235 SFA abrogates platelet production.

236

237 **PUFA-enriched high fat diet prevents platelet reduction**

238 Feeding mice a high fat diet with an enrichment in SFA resulted in decreased platelet counts. This
239 is consistent with our lipidomic data, which revealed a clear bias towards PUFAs, and not SFAs,
240 during thrombopoiesis. Thus, we hypothesized that substituting the SFAs for PUFAs in the high
241 fat diet may prevent obese mice from having reduced platelet counts. To explore this, we first
242 established whether MKs could take up PUFAs, and examined their effect *in vitro* by performing
243 click chemistry as described above. Indeed, MKs dose-dependently incorporated arachidonic acid
244 (Fig. 4a), however it did not significantly alter their area (Fig. 4b) or capacity to form proplatelets
245 *in vitro* (Fig. 4c).

246 To determine whether the low platelet counts observed in the DIO model were a consequence of
247 the high fat diet or the fatty acid saturation status (high SFA), we fed male mice a matched 60%
248 high fat diet enriched in PUFAs (Fig. 4d) instead of SFAs. Mice fed the PUFA diet weighed
249 significantly more than controls (Fig. 4e), but glucose levels were indistinguishable (Fig. 4f). Mice

250 on the high PUFA diet had significantly increased platelet counts after 4 weeks, and platelet
251 counts remained elevated at the study endpoint (Fig. 4g-h). No differences were found in other
252 blood parameters (Extended data Fig. 4a-c) and plasma TPO levels of all mice were within the
253 normal range (Extended Data Table 1). Moreover, there were no differences in platelet lifespan
254 between mice fed chow versus the PUFA-enriched diet (Extended data Fig. 4d).

255 In addition, when assessing the amount of circulating, newly generated reticulated platelets using
256 thiazole orange, we found that mice fed the enriched PUFA diet had a tendency toward more
257 immature platelets in circulation (Fig. 4i-j). Comparable to the DIO mice, MKs in the PUFA-fed
258 mice were significantly larger than the chow group while their number remained unaltered (Fig.
259 4k-l). In addition, their maturation, as measured by ploidy, was substantially enhanced, with a
260 significant decrease in the number of 16n MKs and an increase in 32n MKs (Fig. 4m), suggesting
261 an overall shift to higher ploidy. Together, these data reveal that enhancing the amount of PUFAs
262 in the high fat diet can rescue the reduced platelet counts seen in the DIO model. These results
263 underscore the role of dietary PUFAs in contributing to MK maturation and reveal that
264 supplementation with PUFAs can enhance MK maturation and platelet production.

265

266 **Platelets are unchanged in *Cd36*^{-/-} mice fed high fat diets**

267 Our data revealed that MKs and their progenitors readily take up exogenous fatty acids, and this
268 is an important process during their maturation. Further, modifying dietary fatty acids can directly
269 impact platelet counts *in vivo*. As such, identification of a receptor responsible for fatty acid uptake
270 in MKs and their progenitors is key in understanding the mechanism of how fatty acids impact
271 megakaryopoiesis. As Valet et al. recently demonstrated that MKs can take up fatty acids via the
272 scavenger receptor CD36 to help facilitate membrane maturation¹⁷, and CD36 was upregulated
273 in proplatelet-forming MKs (Fig. 1e), we explored whether CD36 was the mechanism by which
274 MKs and their progenitors incorporate exogenous fatty acids. We utilized a mouse model
275 constitutively lacking CD36 (*Cd36*^{-/-}).²⁰ *Cd36*^{-/-} mice exhibited significantly reduced platelet counts
276 (Fig. 5a).¹⁷ While MPV and IPF remained unchanged, red blood cell counts were also significantly
277 reduced (Fig. 5b). To directly test if CD36-deficient MKs had a defect in taking up fatty acids *in*
278 *vitro*, we used click-chemistry on MKs from *Cd36*^{-/-} and wildtype mice cultured with either the SFA
279 palmitic acid (Fig. 5c-d) or the PUFA arachidonic acid (Fig. 5e). In line with our hypothesis, *Cd36*^{-/-}
280 MKs took up significantly less fatty acids (Fig. 5c), suggesting that the CD36 receptor plays a
281 substantial role in fatty acid uptake of both SFAs (Fig. 5d) and PUFAs (Fig. 5e) in MKs.

282 We next cultured HSPCs derived from *Cd36*^{-/-} and wildtype mice and found a significant decrease
283 in the number of mature MKs that differentiated from HSPCs from *Cd36*^{-/-} mice, suggesting that
284 fatty acid uptake through CD36 is important not only for platelet production but also MK
285 differentiation (Fig. 5f). We examined the number and area of CD41⁺ cells in *Cd36*^{-/-} bone marrow
286 and found no significant reduction (Fig. 5g). Moreover, the ploidy of *in vitro* differentiated MKs
287 was largely unchanged, with only a decrease in the 2n population (Fig. 5h). As *in vitro* MK
288 differentiation was affected in *Cd36*^{-/-} mice, we next characterized proplatelet formation. Critically,
289 CD36-deficient MKs displayed a notable defect in proplatelet formation with both the number of
290 MKs forming proplatelets and proplatelet area being significantly reduced (Fig. 5i-j). This finding
291 strongly suggests that proplatelet formation is dependent on the uptake of essential fatty acids

292 (PUFAS) through CD36. Together, these data indicate that loss of MK CD36 decreases the
293 uptake of both SFAs and PUFAs into MKs in vitro. Further, lack of CD36 on HSPCs decreases
294 their ability to differentiate into MKs and the capacity of MKs to make proplatelets.

295 If CD36 is the receptor that facilitates uptake of fatty acids into MKs and their progenitors in vivo,
296 then mice lacking this receptor would have MKs that are resistant to alterations in dietary fatty
297 acids. Therefore, to test whether the loss of CD36 *in vivo* could disrupt the ability of both SFA-
298 and PUFA-enriched high fat diets to modulate platelet counts, we fed mice chow or 60% high fat
299 diets enriched in either SFAs (DIO model) or PUFAs. Notably, there were no significant
300 differences in platelet counts or platelet production across the mice fed the three different diets
301 after 8 and 13 weeks (Fig. 6 a-f). At week 13, we examined the CD41+ cells in the bone marrow
302 of *Cd36*^{-/-} mice on all diets and found no significant alterations in either MK number or size,
303 consistent with the lack of change in platelet counts (Fig. 6 g-i). This suggests that loss of CD36
304 abrogated the ability of dietary fatty acids to alter MK phenotype and platelet counts in vivo.
305 Together, these data further support the role of CD36 as a key receptor that takes up dietary fatty
306 acids that drive MK maturation and platelet production.

307

308 **Patients with a familial CD36 mutation have thrombocytopenia**

309 To substantiate the biological relevance of CD36 function in platelet production in humans, we
310 identified a family with an idiopathic thrombocytopenia; patients II.1 and II.2 were recruited to the
311 UK-GAPP study (Fig. 7a, Extended data Fig. 6), and clinical histories evaluated. Whole blood
312 cells counts were taken, revealing low platelet counts and high MPV and IPF values (Fig. 7b,
313 Table 1). In addition, the mother (I:2) had bleeding episodes and low platelet counts. Whole
314 Exome Sequencing (WES) analysis was performed on the two patients using a bioinformatic
315 pipeline workflow which identified an average total of 43,884 variants. Genetic variants were
316 filtered against a panel of 358 genes known or predicted to be associated with platelet count,
317 function, or lifespan. These variants were then filtered out by excluding all synonymous and
318 intronic variants followed by excluding all variants with a MAF > 0.01 (Fig. 7c). Pathogenicity
319 prediction of the variants were determined by utilizing the prediction tools (Mutation Taster,
320 PolyPhen-2, SIFT, Provean) and the variants were classified based on the ACMG guidelines.
321 Plausible candidate variants in each patient were then selected based on the pathogenicity
322 prediction (Fig. 7d). A detailed schematic outlining this workflow can be found in Extended data
323 Fig. 6. In both patients II.1 and II.2, we identified a pathogenic heterozygous stop gain variant in
324 exon 10 of the CD36 gene (c.975T>G; p. Tyr325Ter, Fig. 7c).

325 Although this variant has previously been reported at a relatively high frequency (0.08929) in the
326 Afro-Caribbean population compared to the overall population (8.33e-3) and linked to
327 thrombocytopenia²¹, it has not been functionally characterized. Therefore, the relationship
328 between the receptor function and the reported patient phenotype could not be directly discerned.
329 The c.975T>G; p. Tyr325Ter variant was predicted to encode a truncated CD36 protein which
330 lacked the carboxyl-terminal transmembrane domain and potential function of the CD36 protein.
331 Fittingly, western blotting analysis using platelet lysates from the *CD36*-mutation positive patients
332 revealed a truncated band (Fig. 7e). Of note, the tyrosine residue at position 325 is highly
333 conserved across multiple species (Fig. 7f). We modelled the predicted structure of the CD36

334 ectodomain using homology modelling based on Fu-Lien et al.²², showing the absence of a
335 significant portion of the WT CD36 protein as a result of the *CD36* nonsense variant, leading to
336 the truncation and significant loss of domains crucial to the normal functioning of CD36 (Fig. 7g-
337 h). Together, these modeling and experimental data supported the conclusion that the c.975T>G;
338 p. Tyr325Ter mutation led to a truncation of the CD36 protein.

339 We further investigated the function of the CD36 mutant by generating constructs and cloning the
340 wildtype *CD36* cDNA into a pEF-BOS expression vector followed by site-directed mutagenesis to
341 generate 2 mutant forms of CD36: (i) a deletion of the amino acids following the nonsense variant
342 (Tyr325Ter) to the stop codon of the mature protein at amino acid residue 472 and (ii) a
343 substitution of the point mutation only (c.975T>G, p.Tyr325Ter). Initially, the expression of the 3
344 constructs was measured and validated using western blotting, confirming the truncation effect of
345 the 2 mutant CD36 proteins in both Jurkat T cells and HEK293 cells (Fig. 7i). Flow cytometry was
346 then used to probe the expression of CD36 mutant proteins on the cell surface. Of note, only
347 wildtype CD36 and not the mutant constructs, was detected (Extended data Fig. 5a), suggesting
348 that the other constructs were not trafficked to the cell surface. Next, we studied the signaling
349 capacity of the CD36 constructs using a nuclear factor of activated T cells (NFAT)-luciferase
350 reporter assay. The CD36 wildtype protein robustly activated the NFAT-luciferase, while the
351 mutant protein did not, confirming the absence of signaling capacity for the CD36 mutants (Fig.
352 7j). These data are consistent with the flow cytometry data and demonstrate that the mutant CD36
353 protein indeed does not reach the cell surface and does not signal, conferring a complete loss of
354 function in the reported mutation. Together, our data reveal that in both humans and mice, loss
355 of CD36 function results in reduced platelet counts, underscoring its importance in efficient
356 platelet production.

357

358 **Discussion**

359 Through lipidomic analyses, we uncovered an enrichment in PUFAs, essential fatty acids that are
360 primarily diet-derived, throughout MK differentiation and maturation and platelet production. Our
361 data then revealed that fatty acid uptake, functionalization, and metabolism play differing but
362 essential roles in MK differentiation and proplatelet production. Specifically, platelet production
363 from MKs can be modified both in vitro and in vivo by varying the availability of exogenous PUFAs.
364 We demonstrated that CD36 is a key receptor responsible for the uptake of fatty acids in MK
365 progenitors. We further report that a familial loss-of-function mutation in *CD36* results in
366 thrombocytopenia, suggesting that lipid uptake plays a critical role in platelet production.

367 Lipids are a vast class of biomolecules which fulfill three general functions: energy, membrane
368 structure, and signaling.^{4,5} To date, an impressive amount of experimental data has given insights
369 into membrane biogenesis as well as homeostasis and lipid-protein interactions, which paves the
370 way for targeted modification of membrane lipid compositions.²³ In 1987, Dio et al. showed that
371 adding SFAs (palmitic acid, etc.) to a murine fibroblast cell line results in a severe inhibition of cell
372 growth.²⁴ In contrast, increasing the PUFA concentration in liposomes results in a more flexible
373 plasma membrane with a higher deformation rate in response to applied force.²⁵ The idea of
374 enhancing membrane flexibility by modulating PUFA content was further substantiated by Manni
375 et al.¹⁶ Their study revealed that increasing the PUFA content in liposomes results in a higher

376 tubulation rate. This process bears a striking resemblance to proplatelet production, which
377 requires reorganization of the MK membrane system. Our data showed that increasing the dietary
378 SFA:PUFA ratio resulted in a reduction in platelet generation both in vitro and in vivo. One way
379 by which increased SFAs may be reducing proplatelet production is through creating a membrane
380 that is too rigid to accommodate proplatelet extension. Conversely, replacing SFAs with PUFAs
381 may ensure that the MK membrane is sufficiently flexible to allow for both DMS formation and
382 proplatelet production. This is consistent with our lipidomic analysis revealing that MKs and
383 platelets were increasingly enriched in PUFAs. These results highlight the potential to manipulate
384 dietary fatty acid ratios and thereby modify MK phenotype and increase or decrease platelet
385 production in vivo. Ultimately, these approaches may be able to fulfill a significant unmet clinical
386 need by providing ways to modulate thrombopoiesis and mitigate abnormal platelet counts.

387 Changes in exogenous lipid availability and content are associated with a variety of diseases
388 including obesity, which has become a significant health problem worldwide.²⁶ Previous studies
389 have demonstrated that alterations in lipid metabolism and changes in plasma lipid profile are
390 associated with the onset and progression of obesity-related complications.²⁷ Often, however,
391 obesity is associated with a pro-inflammatory and/or pro-thrombotic state that enhances the risk
392 of developing cardiovascular diseases, where platelets play a well-established pathogenic role.²⁸⁻
393 ³⁰ In these settings, it is challenging to study the impact of obesity and an altered plasma lipid
394 profile on MKs and platelets independent of comorbidities such as inflammation.^{31,32} Recently, a
395 new subset of obese individuals classified as 'metabolically healthy obese' (MHO) were found to
396 be protected against worsening metabolic health.^{33,34} Despite the debate about the use and
397 clinical implications of MHO as a diagnosis, obesity without cardiometabolic abnormalities may
398 provide a unique human model system to study mechanisms linking different diets and fat
399 accumulation to obesity-related cardiometabolic complications.³³ To date, no studies have
400 reported how MHO may impact megakaryopoiesis or platelet production in humans. However,
401 our in vitro data suggest that changes in plasma lipid content alone may lead to changes in MK
402 maturation and platelet production, even in the absence of inflammation or other comorbidities
403 associated with obesity. Notably, depending on the lipid profile, our data suggest that these
404 changes may not always be pathogenic. Further, these data set the stage for future studies
405 examining how changes in dietary lipids might also modify platelet function and reactivity.

406 CD36 is a multifunctional protein; one of its roles is to accelerate exogenous fatty acid uptake and
407 incorporation into more complex lipids.^{35,36} Here, we substantiated CD36 as a key receptor for the
408 uptake of fatty acids in MKs and their progenitors and revealed that loss of CD36 led to reduced
409 platelet counts in both mice and humans. These findings align with recent studies that
410 demonstrate fatty acid uptake transfer between adipocytes and MKs is dependent on CD36.¹⁷
411 Notably, evidence suggests that there is little expression of CD36 on HSCs, but expression
412 increases dramatically in MKs³⁷, providing a possible mechanism for how they rapidly accumulate
413 fatty acids over maturation via a cell intrinsic manner.

414 There are also important limitations to this work that should be noted. First, our lipidomic results
415 reflect total lipids, and membrane lipids do not distinguish between the plasma/demarcation
416 membrane and organelle membranes. Additionally, we only identified and characterized two
417 patients with the c.975T>G, p.Tyr325Ter *CD36* mutation. There have been various *CD36*
418 mutations identified, some of which have been associated with thrombocytopenia.^{21,38} Notably,

419 many of these mutations have not been functionally characterized, making their relationship with
420 platelet counts hard to interpret because it is unknown how each mutation affects CD36 receptor
421 activity. In addition, the fact that *Cd36*^{-/-} mice and humans with mutated or absent CD36 have
422 both MKs and platelets, albeit at reduced levels, suggests that other receptors, such as the free
423 fatty acid receptors (FFARs) are also involved in fatty acid uptake.³⁹ Specifically, FFAR₂ may be
424 a plausible candidate as it is expressed in MKs and their precursor cells.⁴⁰

425 In summary, our data provide unique insights into the functional role of lipids, diet, and lipid
426 metabolism during MK differentiation, maturation, and platelet production. We have further
427 validated an essential receptor, CD36, as a key mechanism for lipid uptake and identified a *CD36*
428 mutation that is a genetic determinant of thrombocytopenia and pathological bleeding. In the
429 future, we aim to identify additional MK-specific lipid signatures to determine different ways to
430 increase or decrease megakaryopoiesis and platelet production. This could be as simple as
431 altering fatty acid ratios in the diet or involve therapeutics that target key fatty acid biosynthesis
432 enzymes or the uptake receptor CD36. Ultimately, these approaches may be able to meet a
433 significant unmet clinical need in the modulation of thrombopoiesis to mitigate abnormal platelet
434 counts.

435

436 **Methods**

437 **Animal Models**

438 CD-1 and C57BL/6J mice were acquired from Charles River Laboratories (Worcester, MA) or The
439 Jackson Laboratory (Bar Harbor, ME). Mice were housed in the animal facilities at Boston
440 Children's Hospital, Boston, MA or Michigan State University, East Lansing, MI. All animal work
441 was approved by the international animal care and use committee at Boston Children's Hospital,
442 Boston, MA (Protocols 00001248 and 00001423) and Michigan State University
443 (PROTO201800186). In all terminal experiments, mice were sacrificed using methods consistent
444 with IACUC protocol guidelines.

445 For experiments with high fat diets, adult C57BL/6J and *Cd36*^{-/-} mice were placed on the following
446 diets: 1) Research diets Inc. D12492, Rodent Diet With 60 kcal% from fat and 2) Research diets
447 Inc. D22050406i, Rodent Diet with 60 Kcal% Fat enriched in polyunsaturated fatty acids. As a
448 control, mice were fed a chow diet (D12450B, Research diets Inc.). Mice received water and food
449 ad libitum. Mice were sacrificed at the indicated endpoints using methods consistent with IACUC
450 protocol guidelines. *Cd36* knockout mice (*Cd36*^{-/-}) were obtained from The Jackson Laboratory
451 (Strain #019006). Homozygous mice were bred to maintain a colony of knockout mice. Ear
452 clipping specimens were sent to Transnetyx, Inc for genotyping to ensure integrity of the strain
453 and preservation of the *Cd36* gene knockout.

454

455 **Blood cell characterization**

456 For non-terminal blood collection, mice were anesthetized with isoflurane and 70 μ L of blood
457 collected from the retro-orbital capillary bed using heparinized capillaries and transferred into
458 EDTA-coated tubes (BD Microtainer™ Capillary Blood Collector). Platelet count, size, and basic
459 blood parameters were obtained using an automated cell counter (XN-1000™ Sysmex).

460

461 **Thiazole Orange analysis**

462 Whole blood (5 μ L) was diluted in 500 μ L Tyrode's buffer. 50 μ L of diluted blood was incubated
463 with 200 ng mL⁻¹ of thiazole orange (TO) and an antibody against CD41/61 (Emfret Analytics) was
464 used to identify platelets. TO-positive platelets were identified by flow cytometry (Accuri C6 plus,
465 BD Biosciences).

466

467 **Platelet Isolation**

468 For terminal bleeds, mice were anaesthetized using 2% isoflurane and blood was collected from
469 the inferior vena cava into EDTA containing tubes. Platelet-rich plasma (PRP) was obtained by
470 centrifugation at 200g for 10 minutes (acceleration 9, break 6). After addition of PGI1 (final
471 concentration 560 nM, P5515 Sigma) and Apyrase (final concentration 0.02 U/mL, A6123-500U
472 Sigma), PRP was spun down at 800g for 10 minutes (acceleration 9, brake 6). Platelets were
473 washed twice in modified Tyrode's buffer (134 mM NaCl, 2.9 mM KCl, 20 mM HEPES, 1 mM
474 MgCl₂, 5 mM Glucose, pH 6.5) containing PGI1 and Apyrase (10 min at 800g with acceleration 9
475 and break 6). After the last wash, the platelet pellet was resuspended in modified Tyrode's buffer.

476 Platelets were counted on the ProCyte Dx and diluted in PBS to a final concentration of 10,000
477 platelets/ μ L. Samples were stored at -80°C prior to lipidomics studies.

478

479 **Platelet lifespan**

480 Fifty mg of MilliporeSigma™ Calbiochem™ Biotin-NHS, Water-Soluble (Cat: 20-311-8) was
481 injected intravenously into each mouse. At the indicated time points, 50 μ L of blood was collected
482 and incubated with 1 μ L Streptavidin (Alexa Fluor™ 488 Conjugate, Invitrogen, Cat: S11223) and
483 1 μ L PE-conjugated anti-CD41 antibody (BioLegend, Cat:133906) for 10 minutes at room
484 temperature. The percentage of double positive platelets was determined by flow cytometry
485 (Accuri C6 plus, BD Biosciences). Platelet lifespan was determined by measuring the percentage
486 of biotin-labeled platelets over time.

487

488 **Isolation of murine fetal liver-derived MKs**

489 Fetal liver-derived MKs were cultured from fetal livers as previously described.⁴¹ Briefly, pregnant
490 CD-1 mice at day 13.5 of gestation mice were sacrificed by CO_2 asphyxiation followed by cervical
491 dislocation and fetal livers were extracted. Homogenized fetal liver cells were then cultured in
492 complete media (Dulbecco's Modified Eagle Medium (Sigma), 10% Fetal Bovine Serum, (Sigma)
493 and 1% Penicillin Streptomycin (Gibco)) in the presence of recombinant murine thrombopoietin
494 (50 ng/mL) for 4 days. On day 4, mature MKs were enriched using a bovine serum albumin (BSA)
495 density gradient.

496

497 **Isolation of murine bone marrow-derived MKs**

498 Mice were sacrificed and long bones and iliac crests were isolated and bone marrow was obtained
499 by centrifugation at 2500g for 40s as previously described.⁴² HSPCs were separated by lineage
500 depletion using an antibody mixture (Lineage depletion panel, 133307, Biolegend) and magnetic
501 beads (CD4 untouched, 11415D, Invitrogen). For MK maturation, HSPCs were incubated in
502 complete medium containing TPO (50 ng/mL) and recombinant hirudin (100 U/mL, Aniara
503 Diagnostics, RE120A) for 4 days.⁴³ Differentiated MKs were enriched using a BSA density
504 gradient.

505

506 **HSPC panel**

507 Mice were sacrificed, long bones and iliac crests isolated, and bone marrow was obtained by
508 centrifugation as described above. Bone marrow cells were filtered using a 70 μ m PluriStrainer
509 filter (Pluriselect). Red blood cell lysis was performed according to the manufacturer's instructions
510 (Lysis Buffer, 555899, BD Biosciences). Cells were stained as follows:

511 For each sample, 1 μ L of each antibody (1:100) and 50 μ L of BV staining buffer was added. The
512 antibodies used were the following: Pacific Blue™ anti-mouse Lineage Cocktail with Isotype Ctrl
513 (Clones 17A2; RB6-8C5; RA3-6B2; Ter-119; M1/70, (Biolegend, 133305)), APC CD117 (c-Kit)
514 Monoclonal Antibody (clone 2B8, eBioscience™, 17-1171-82), PerCP/Cyanine5.5 anti-mouse Ly-6A/E

515 (Sca-1) Antibody (clone D7, Biolegend 108123), Brilliant Violet 605™ anti-mouse CD41 Antibody
516 (clone MWReg30, Biolegend 133921), APC/Cyanine7 anti-mouse CD48 Antibody (clone HM48-
517 1, Biolegend 103432), BD OptiBuild™ BV786 Rat Anti-Mouse CD34 (clone RAM34, BD
518 Bioscience 742971), PE/Cyanine5 anti-mouse CD150 (SLAM) Antibody (clone TC15-12F12.2,
519 115912), BD Pharmingen™ PE Rat Anti-Mouse CD13 (clone R3-242, BD Bioscience 558745),
520 PE/Cyanine7 anti-mouse CD105 Antibody (clone MJ7/18, Biolegend 120409).
521 Unstained samples from both groups, single stained samples, single color beads (1 µL of antibody
522 and 1 drop of UltraComp eBeads Plus Compensation Beads, Invitrogen), and FMO controls were
523 used. Cells were stained for 30 min, followed by 2 consecutive washes with MACS running buffer
524 (Miltenyi). Prior to measuring the sample, DAPI (150 nM) was added, and cells were filtered using
525 a 70 µm PluriStrainer filter. Samples were analyzed using a Spectral Flow Cytometry, Cytex
526 Aurora (Cytexbio). Gating strategies are shown in Extended data Figure 6.
527

528 **Cell sorting for lipidomics**

529 Bone marrow cells were filtered using a 100 µm filter (Pluriselect). Red blood cell lysis was
530 performed according to the manufacturers' instructions (Lysis Buffer, 555899, BD Biosciences).
531 MEP (Lin-, Sca-1, c-Kit+, CD34-, FcγR-, 10,000 cells) and MK (immature: CD41+, and mature:
532 CD41+/CD42d+ double positive, 10,000 cells) populations were isolated using fluorescence
533 activated cell sorting according to published studies.⁴⁴ Samples were sorted using a BD FACS
534 Aria III (BD bioscience).

535

536 **Lipid extraction**

537 Cell samples were lyophilized using either a Savant SpeedVac (Thermo Scientific) or a CoolSafe
538 freeze dryer (ScanVac) prior to extraction and resuspended in 10 µL MilliQ H₂O. Lipids were
539 extracted using a modified single-phase chloroform/methanol extraction method.⁴⁵ Briefly, 200 µL
540 chloroform-methanol (2:1) was added to each sample along with an internal standard (ITSD)
541 mixture containing stable-isotope labelled or non-physiological lipids. In tandem, blank control
542 samples and plasma QCs were extracted and dispersed evenly throughout the extraction order
543 to ensure optimal assay performance and to monitor variation that may arise from the extraction.
544 Samples were subsequently mixed with a rotary mixer for 10 mins at 1g, sonicated for 30 mins at
545 room temperature and centrifuged at 11,337g for 10 mins to precipitate proteins from the lipid
546 extracts. Supernatant containing the extracted lipids were transferred to a 96 well plate and
547 evaporated using a Savant SpeedVac. Once dried, extracts were reconstituted in H₂O-saturated
548 butanol and methanol with 10 mM ammonium formate and moved to glass vials and stored until
549 mass spectrometry analysis.

550

551 **Liquid chromatography tandem mass spectrometry (LC-MS/MS)**

552 Lipid extracts were analyzed using an Agilent 6490 triple quadrupole (QqQ) mass spectrometer
553 coupled to an Agilent 1290 high performance liquid chromatography (HPLC) system as previously
554 published⁴⁶. Briefly, we used a ZORBAX eclipse plus C18 column (2.1x100mm 1.8µm, Agilent)
555 with thermostat set to 45°C. The final mass spectrometry analysis on each cell population was

556 performed in positive mode with dynamic scheduled MRM. Solvents consisted of solvent A (50%
557 H₂O, 30% acetonitrile, 20% isopropanol with 10 mM ammonium formate) and solvent B (1% H₂O,
558 9% acetonitrile, 90% isopropanol with 10 mM ammonium formate) and followed a modified 20-
559 minute gradient as shown in **Supplementary Table 1**.

560 A wash vial comprising of 1:1 butanol:methanol was used after each sample injection. To further
561 improve chromatic peak shape for many anionic/acidic lipid species (notably PS, PA, PIP, S1P),
562 an additional pre-run passivation step was done with phosphoric acid to minimize interaction
563 between the HPLC unit and these lipids. The m/z pairs used for each lipid species can be found
564 in **Supplementary Table 2**.

565

566 **Lipid nomenclature**

567 The lipid names used follow guidelines set by the LIPIDMAPS consortium.⁴⁷ Phospholipids with
568 detailed characteristics i.e., acyl chain composition are annotated as [PC(16:0_20:4)] with PC
569 being the lipid class and (16:0_20:4) representing the acyl chains found on the glycerol backbone,
570 irrespective of sn1 or sn2 position. Lipids without specific structural annotations are named based
571 on their sum acyl chain length and degrees of saturation e.g. PC (36:4). Isomeric lipid species
572 separated chromatographically but incompletely annotated were designated (a), (b) etc., with (a)
573 and (b) representing elution order. Owing to technical limitations, we were unable to assign acyl
574 chains to a specific sn1 or sn2 position for the majority of PL species, only that the acyl chain was
575 present at either the sn1 or sn2 position. In the case of ether-PC and PE, the alkyl or alkenyl
576 chains were always located at the sn1 position and the acyl chain always at the sn2 position. In
577 addition, we were unable to determine acyl chain composition for all PLs and the data shown
578 therefore represents those PLs for which we were able to obtain information on their structural
579 composition. Notably, this represents >90% of total PLs for all cell types.

580

581 **Analysis of lipids**

582 Individual analyte areas were divided by the area of the corresponding internal standards (ITSDs),
583 and the median of ITSD containing blank samples was subtracted from each analyte (background
584 subtraction). Background subtracted values were multiplied by the concentration of the ITSD and
585 the analyte's respective response factor (Rf). Zeroed background subtraction values (i.e., sample
586 values which were lower than the median blank + ITSD samples) were replaced with 1/10th of
587 the minimum value for the corresponding analyte. Data was ultimately normalized to pmol/μmol
588 of total lipidome where background subtracted data for an individual lipid was divided by the sum
589 of the total lipidome of the sample and multiplied by a factor of 10⁶. This allowed us to interrogate
590 the lipid composition of the cellular membrane independently of cell size and protein content.
591 Accurate normalization to protein content was not feasible due to the small rare cell populations
592 and small sample sizes.

593 tSNE plots were generated in R version 3.6.2 (AN). The data points were initially log₁₀
594 transformed and unit variance is scaled. The pairwise distances were computed to determine the
595 similarity between the data points followed by the calculation of the probability distribution for each
596 data point. Following data optimization, the data points are plotted creating a visual presentation

597 of the structure of the high-dimensional data, with similar points appearing close together in the
598 plot. Normalized raw data can be found in supplemental data.

599

600 **Lipid Enrichment Analysis**

601 Lipid ontology analysis was performed using Lipid Ontology (LION). Analysis was conducted in
602 ranking mode with lipidomic data normalized to mol%. LION-term enrichment was considered
603 significant when FDR q value < 0.05.

604

605 **RNAseq dataset and Enrichment Analysis**

606 The mRNA seq dataset was previously published by our group.¹⁹ To corroborate if lipid-related
607 genes were differently regulated in non-proplatelet-forming MKs vs proplatelet-forming MKs, the
608 dataset was examined for keywords (e.g lipid, phospholipid, coA, fatty acid, CD36). Selected
609 genes with p value and fold change were plotted using Prisma. Enrichment analysis was done
610 using Reactome.⁴⁸

611

612 **Flow cytometry on cultured MKs**

613 At day 4 of maturation, MK cultures were centrifuged and washed with autoMACS® Running
614 Buffer (130-091-221, Miltenyi). Cells were stained for 30 min using CD41-FITC (133904,
615 BioLegend) and CD42d-APC (148506, BioLegend) antibodies. Unstained and single cell controls
616 were included. After the incubation, cells were washed twice and analyzed on a FACScalibur (BD
617 Biosciences). The percentage of CD41- and CD41/CD42d-positive cells was analyzed using
618 FlowJo and normalized to the vehicle.

619

620 **Cytotoxicity assay**

621 The lactate dehydrogenase (LDH) cytotoxicity assay was performed according to the
622 manufacturers' instructions (C20300, ThermoFisher Scientific). Mature FLMKs were treated with
623 indicated dosages of Triacsin C (T4540, Sigma), PF-05175175 (PZ0299, Sigma), and Cerulenin
624 (C2389, Sigma) and incubated overnight in a 96-well-plate and LDH activity in the supernatant
625 was measured. As a positive control, cells were lysed with TritonX-100. MKs treated with vehicle
626 were treated as a negative control (baseline).

627

628 **Analysis of proplatelet formation using the Incucyte automated microscope**

629 Fetal liver- or bone marrow-derived MKs were isolated by density gradient as described above.
630 MKs were either untreated, supplemented with different fatty acids, or treated with inhibitors
631 (Triacsin C, T4540, Sigma), PF-05175175 (PZ0299, Sigma), Cerulenin (C2389, Sigma), as
632 indicated. For supplementation, MK were treated with palmitic acid (P0500, Sigma) or arachidonic
633 acid (A-122, Sigma) in serum-free media. Proplatelet formation was visualized on the Incucyte

634 imaging system and quantified using a custom image analysis pipeline or manually by counting
635 the percentage of MKs making proplatelets, using Image J, as described.⁴⁹

636

637 **Immunostaining of proplatelet-forming MKs**

638 Bone marrow HSPCs were cultured as described above and MKs isolated by density gradient
639 enrichment. MKs were treated with inhibitors or supplemented with different fatty acids as
640 indicated (see below). After treatment, cells were pipetted gently onto the bottom of a μ -side 8-
641 well Ibidi chamber coated with an anti-CD31 antibody (102502, BioLegend) and incubated
642 overnight. The following day, cells were fixed using 4% PFA containing 0.1% Tween20 for 30 min,
643 followed by 3% BSA, and stained for α -tubulin (A488, 322588, ThermoFisher), F-actin (Phalloidin-
644 Atto647N, A22287), and DAPI (Sigma) overnight. Proplatelet formation was visualized using a
645 Zeiss LSM880 confocal microscope (40x objective).

646

647 **Oxygen Consumption Measurement**

648 MKs were suspended in XF base medium DMEM (Agilent Bioscience) supplemented with 1 mM
649 sodium pyruvate (Agilent Bioscience), 2 mM glutamine (Wisent), and 10 mM glucose (Agilent
650 Bioscience), pH 7.4. A total of 10,000 MKs per well was seeded on XF-96 plates
651 (Agilent/Seahorse Bioscience). Cells were treated with Triacsin C (T4540, Sigma), PF-05175175
652 (PZ0299, Sigma), or Cerulenin (C2389, Sigma) at the indicated concentrations in complete media
653 for 90 min prior to measurement. Plates were then centrifugated at 300g for 2 min at room
654 temperature. We ensured cell homogeneous repartition under a microscope and plates were
655 maintained at 37°C without CO₂ for approximately 60 min prior to loading. Oxygen consumption
656 rates were measured in accordance with manufacturer instructions (Agilent/Seahorse
657 Bioscience). Experiments were replicated in three to five wells and averaged for each
658 experimental condition. A total of 3 measurements of oxygen consumption for each condition
659 were made approximately every 10 min (mix for 3 min, wait for 4 min and measure for 3 min)
660 under basal conditions and after sequential injection of oligomycin (4 μ M), FCCP (carbonyl
661 cyanide 4-(trifluoromethoxy) phenylhydrazone, (1 μ M) and rotenone/antimycin A (1 μ M each).
662 Oligomycin is used as an ATP synthase inhibitor, FCCP as an uncoupling agent of oxidative
663 phosphorylation, rotenone as a complex I inhibitor, and antimycin A as a complex III inhibitor. This
664 allowed us to estimate the contribution of individual parameters for basal respiration, proton leak,
665 maximal respiration, spare respiratory capacity, non-mitochondrial respiration, and ATP
666 production.

667

668 **Lipid incorporation through click-chemistry**

669 HSPCs were isolated as described above. After lineage depletion, cells were supplemented with
670 fatty acids modified with a ω -terminal alkyne group (Palmitic acid, 13266; Arachidonic Acid,
671 10538; Cayman Chemical). After 4 days of maturation, click-chemistry was performed using
672 green-fluorescent Alexa Fluor® 488 azide (C10641, ThermoFisher Scientific) according to the
673 manufacturers' instructions. Azides are specifically reactive with terminal alkynes via a copper-

674 catalyzed click reaction.^{50,51} Cells were image using a Zeiss LSM880 confocal microscope (20x
675 and 63x objectives). For analysis, Alexa Fluor® 488 MFI was measured using Image J and
676 normalized to vehicle.

677

678 **MK ploidy analysis**

679 Bone marrow was isolated from 1 femur by centrifugation at 2500g for 40 seconds. Cells were
680 filtered through a 100 µm cell strainer and red blood cells were lysed using ACK buffer (A1049201,
681 Gibco). Cells were washed in PBS, fixed, and permeabilized in 100% ethanol for 30 min on ice.
682 Cells were treated with RNase A (EN0531, ThermoFisher Scientific) and stained with an anti-
683 CD41-FITC antibody (133904, BioLegend) and propidium iodide (P1304-MP, Sigma Aldrich) for
684 30 min on ice. Ploidy distribution and percentage of CD41-positive cells were quantified by flow
685 cytometry (BD AccuriC6 Plus).

686

687 **Cryosectioning and immunofluorescence staining**

688 Mice were sacrificed and femurs isolated and fixed in 4% PFA overnight. Femurs were transferred
689 into 10% sucrose in PBS and a sucrose gradient was performed over 3 days. Femurs were
690 sectioned at 10 µm using a Cryostat CM3050 S (Leica Biosystem), transferred onto slides using
691 a tape-transfer system⁵², and rehydrated in PBS for 15 min. Sections were blocked using 5% goat
692 serum and stained using antibodies against CD41 (133902, Biolegend) and laminin (L9393,
693 Sigma) overnight. The following day, sections were incubated with secondary antibodies (goat
694 anti-rat A488 and goat anti-rabbit A647, respectively). After washing in PBS containing 0.1%
695 TritonX 100, DAPI was added for 5 min and the slides were mounted using Fluoroshield (Sigma
696 Aldrich). Image acquisition was performed using a 20x objective (Zeiss LSM880). MK number
697 and area were quantified manually using ImageJ Software (NIH).

698

699 **Patient recruitment and testing**

700 Patients were consented and recruited to the GAPP study from multiple collaborating Hemophilia
701 Centers across the UK and Ireland as previously described⁵³ and approved by the UK National
702 Research Ethics Service by the Research Ethics Committee of West Midlands (06/MRE07/36).
703 The study cohort currently consists of >1000 patients with a history of bleeding and suspected of
704 having a platelet disorder of unknown cause. Platelet counts, mean platelet volume (MPV) and
705 other hematological parameters were measured on the Sysmex Whole Blood Analyzer. Whole
706 exome sequencing (WES) was performed in patient genomic DNA as previously reported.⁵⁴ For
707 WES filtering of candidate genetic variants was performed to identify rare variants and final
708 sequence variants were confirmed in patients using Sanger sequencing.

709

710 **Candidate gene panel analysis**

711 Whole exome sequencing analysis was carried out using the bioinformatic pipeline workflow
712 which identified an average of 38,812 variants per individual sample. The bioinformatic pipeline

713 was used to refine the variants using a series of filtering steps as displayed in Extended data Fig
714 6. The variants were filtered against a panel of 358 genes known or predicted to be associated
715 with platelet count, function, or lifespan. On average, 222 variants from the gene panel were
716 identified per individual. These variants were then filtered, excluding all synonymous and intronic
717 variants followed by excluding all variants with a MAF of more than 0.01. On average, 16
718 sequence variants with a MAF of ≤ 0.01 were noted among patients in the panel of 358 platelet
719 related genes. Pathogenicity of the variants was predicted by utilizing the prediction tools
720 (Mutation Taster, PolyPhen-2, SIFT, Provean) and the variants were classified based on the
721 ACMG guidelines. This gave an average of 9 sequence variants per patient. The resulting
722 sequence variants are shown in Extended Data Table 2.

723

724 **Functional analysis of CD36 mutants and expression**

725 The Q5 Site-Directed Mutagenesis (SDM) Kit (NEB®, USA, #E0554S) was used to introduce the
726 *CD36* heterozygous stop gain variant (c.975T>G; p. Tyr325Ter) into the human *CD36* cDNA wild-
727 type cloned into the mammalian expression pEF-BOS⁵⁵ using the following primers:

728 SDM_CD36 F_Deletion 5'- GTATGTACCAAAAAATATTGCTTC
729 SDM_CD36 R_Deletion 5'- CTATGATGTACAATTTTTTGAGATAATTTTTTC
730 SDM_CD36 F_Substitution 5'- GTACATCATAGGGTGTGCTAG
731 SDM_CD36 R_Substitution 5'- AATTTTTTGAGATAATTTTTTCTGTG

732 Jurkat T (TIB-152) and HEK293 (CRL-1573) were purchased at American Type Culture Collection
733 (ATCC). The NFAT-luciferase reporter assay was used as previously described.⁵⁶ Briefly, Jurkat
734 T cells were electroporated with 20 μ g NFAT-luciferase construct and 12.5 μ g of either wildtype
735 *CD36* or mutant *CD36* constructs. Twenty-four hours post transfection, cells were harvested and
736 purified, and flow cytometry and western blot analyses were used to assess expression levels.

737

738 **Statistics and Reproducibility**

739 The results are presented as mean \pm standard deviation (SD). Data distributions were analyzed
740 using the Shapiro-Wilk-test and differences between control and mutant mice were statistically
741 analyzed using unpaired, two-tailed Student's t-test, and one- or two-way ANOVA. Tukey, Dunnett
742 or Sidak's post-hoc tests were used for multiple comparisons, as indicated. P-values < 0.05 were
743 considered statistically significant. For representative images, each experiment was repeated
744 three times independently, with equivalent results.

745

746 **Data Availability**

747 All data supporting the findings in this study are included in the main article and associated files.
748 Source data are provided with this manuscript. All raw lipidomics data can be found at:
749 <https://www.ebi.ac.uk/metabolights/MTBLS8042>

750

751 **Code Availability**

752 Instructions and code for the automated pipeline analysis of proplatelet production from
753 megakaryocytes can be found at: <https://github.com/broadinstitute/Italiano-MK-Analysis>

754

755 **Acknowledgements**

756 This work is supported by: the National Institutes of Health, National Institute of Diabetes and
757 Digestive and Kidney Diseases (R03DK124746 to KRM, R01DK112778 to JPL) and National
758 Heart, Lung, and Blood Institute (R01HL151494 to KRM, 5T32HL007734 to TH, R35HL161175
759 to JEI), fellowships from the American Society of Hematology (ASH Restart Award to MNB) and
760 the American Heart Association (23POST1011433 to MNB), a Walter Benjamin Fellowship from
761 the German Research Foundation (DFG; BE 7766/2-1 to ICB), the Boston Children's Hospital
762 Surgical Foundation (TH and MP), the Wellcome Trust (218649/Z/19/Z to AOK), the Saudi Arabia
763 Cultural Bureau in London (IA), the National Health and Medical Research Council of Australia
764 (APP1194329 to AJM and Investigator Grant 2009965 to PJM), the Fonds de Recherche en Santé
765 du Québec and Canadian Institutes of Health Research (EB), and the US Department of
766 Agriculture (USDA) National Institute of Food and Agriculture (to JPL).

767 We would like to thank Drs. Connie Koo and Mike Tomlinson from the University of Birmingham
768 (Birmingham, UK) for assistance with *in vitro* characterization of the CD36 mutation and Dr
769 Beatrice Nolan (Trinity College Dublin) for referring the patients to the GAPP study. We would
770 also like to thank Dr. Mathieu Laplante (University of Laval, Quebec, CA) and his team for their
771 help with experiments and for being an excellent collaborator. Thank you to Dr. Jessica Cardenas
772 (The University of Texas Health Science Center at Houston) and Dr. Luis Batista (Washington
773 University in St. Louis) for their critical review of the manuscript, excellent edits, and support
774 during the publishing process.

775

776 **Author Contributions Statement**

777 MNB conceived the study, performed experiments, collected, interpreted, and analyzed data, and
778 wrote the manuscript. GP, ICB and IA performed experiments, collected, and analyzed data. AOK
779 provided intellectual input. EC designed and developed image analysis methodologies. DJG, DF,
780 KG, ZW and IA performed experiments and analyzed data. TH and MP maintained the CD36
781 knockout mouse colony. JPL performed experiments and analyzed data. NVM recruited and
782 governed the patient's ethics, performed experiments, analyzed data, and helped to draft the
783 manuscript. PJM and TJC analyzed data and prepared figures. NAM performed experiments and
784 analyzed data. PJM and JEI provided intellectual input and key reagents. EB provided intellectual
785 input and interpreted data. AJM helped conceive the lipidomic study, interpret the data, and write
786 the manuscript. KRM conceived and directed the study, analyzed and interpreted data, and wrote
787 the manuscript.

788 All authors provided input on and reviewed the manuscript.

789

790 **Competing Interests Statement**

791 JEI has financial interest in and is a founder of StellarBio, a biotechnology company focused
792 on making donor-independent platelet-like cells for regenerative medicine. The interests of JEI
793 are managed by Boston Children's Hospital.

794 All other authors have no conflicts of interest to declare that are relevant to the content of this
795 article.

796

797

798 **Tables**

799

800 **Table 1. Patient details and hematologic parameters.** Haematologic parameters of patients
 801 II.1 and II.2. M: male, F: female, WBC: white blood cell, RBC: red blood cell, Mono: monocyte,
 802 IPF: immature platelet fraction, MPV: mean platelet volume. MPV values were shown in the table
 803 as (Large) because platelets with large volume are undetectable by the Sysmex analyser. The
 804 Sysmex blood cell analyser showed the hematologic parameter normal ranges which were taken
 805 from ⁵⁷.

806

Patient	II.1	II.2	Normal range
Age	12-16	12-16	—
Sex	M	F	—
WBC	3.55	5.01	M 3.91 – 10.90 x10 ⁹ /L F 4.49 – 12.68
RBC	4.73	3.87	M 4.44 – 5.61 x10 ¹² /L F 3.92 – 5.08
Monocytes	0.28	0.32	M 0.29 – 0.95 x10 ⁹ /L F 0.25 – 0.84
Platelets	79	87	M 166 – 308 x10 ⁹ /L F 173 - 390
IPF	24.4	36.8	M 0.8 – 6.3 % F 0.8 – 6.2
MPV	Large	Large	M 9.3 – 12.1 fL F 9.1 – 11.9

807

808

809

810

811

812

813

814

815

816

817

818

819

820

821

822

823

824 **Figure Legends**

825

826 **Figure 1. Megakaryocytes and platelets have a unique lipid profile that is enriched in**
827 **polyunsaturated fatty acids.** (a) Murine bone marrow cell populations were isolated by
828 fluorescence-activated cell sorting and platelets by sequential centrifugation. Lipids were
829 extracted and analyzed using 20-min gradient HPLC and mass spectrometry (see methods for
830 details), n=8 for MEP and n=4 for all other cell populations. (b) T-distributed stochastic neighbor
831 embedding analysis (tSNE) highlights lipidomic differences between MEPs, immature (CD41+)
832 MKs, mature (CD41/42+) MKs, and platelets. (c) LION enrichment analysis showing the top 10
833 upregulated LION terms. (d) Bulk RNA sequencing was performed on MKs immediately preceding
834 and during proplatelet formation¹⁹ and heatmap shows the log₂FoldChange of selected genes.
835 (e) Reactome enrichment analysis from bulk RNA sequencing on MKs reveals that canonical
836 pathways altered include metabolism of lipids, synthesis of very long-chain fatty acyl-CoAs, and
837 fatty acyl-CoA biosynthesis. Color intensity is directly correlated to the false discovery rate. Total
838 percentage of (f) phospholipid classes and (g) lipid saturation levels of indicated murine bone
839 marrow cell populations in lipidomics analyses. Percentage of SFAs (h) and PUFAs with 6+
840 double bonds (i) in indicated cell populations. MEP, n=8 biologically independent samples; CD41+
841 MKs, CD41/CD42+ MKs and platelets, n=4 biologically independent samples. One-way ANOVA,
842 Tukey's multiple comparison test. Data are presented as mean +/- SD. Illustrations were done
843 using Biorender®

844 *MK: megakaryocyte; MEP: MK-erythroid progenitor; PA: phosphatidic acid; PC:*
845 *phosphatidylcholine; PE: phosphatidylethanolamine; PI: phosphatidylinositol; PS:*
846 *phosphatidylserine; PG: phosphatidylglycerol; SFA: saturated fatty acid; MUFA:*
847 *monounsaturated fatty acid; PUFA: polyunsaturated fatty acid*

848

849 **Figure 2. Fatty acid incorporation and de novo lipogenesis are necessary for MK**
850 **differentiation and efficient proplatelet formation.** (a) Schematic of fatty acid functionalization
851 through long chain acyl-coA synthetase (ACSL). Murine bone marrow HSPCs were cultured with
852 TPO and treated with the ACSL inhibitor Triacsin C (1µM and 3µM). (b) Representative images
853 after 4 days of treatment, showing MKs (large cells) and surrounding HSPCs. n=5, scale bar=150
854 µm (c) CD41+ and CD41/CD42d+ cells were quantified using flow cytometry, n=5, one-way
855 ANOVA – Dunnett's test (d) Schematic of *de novo* lipogenesis. Murine bone marrow HSPCs were
856 cultured with TPO and treated on day 0 with the acetyl-CoA carboxylase (ACC) and fatty acid
857 synthetase (FASN) inhibitors, (e) PF-05175157 (0.3 and 1 µM) n=4, one-way ANOVA – Dunnett's
858 test, and (f) Cerulenin (1 and 3 µg/mL) n=6, respectively. Cells were quantified by flow cytometry,
859 one-way ANOVA – Dunnett's test. Data are presented as mean +/- SD (g) Mature fetal liver MKs
860 (day 4) were treated with inhibitors at indicated dosages and percentage of MKs making
861 proplatelets and proplatelet area were quantified using the Incucyte high content imaging system.
862 (h) Representative phase contrast image showing example quantification of round (red outline)
863 versus proplatelet-making (green outline) MKs (vehicle, left, and Triacsin C, 3 µM, right). (i)
864 Representative graph of vehicle (grey) and Triacsin C (1 and 3 µM, dark and light yellow,
865 respectively), n=3, Two-way Anova. Data are presented as mean +/- SEM (connecting bars) (j)
866 Representative images of vehicle (left), Triacsin 3µM, (right). b-tubulin (cyan), phalloidin
867 (magenta), DAPI (blue). Scale bar=50 µm (k) Representative graph of vehicle (grey) and ACC
868 inhibitor, PF-05175175 (0.1 and 0.3µM, dark and light green, respectively), n=3, Two-way Anova.
869 Data are presented as mean +/- SEM (connecting bars), (l) Representative images of vehicle (left),
870 PF-05175175 1µM, (right). b-tubulin (cyan), phalloidin (magenta), DAPI (blue). Scale bar=50 µm.

871 (m) Representative graph of vehicle (grey) and FASN inhibitor, cerulenin (1 and 3 $\mu\text{g}/\text{mL}$, dark
872 and light pink, respectively), $n=3$, Two-way Anova. Data are presented as mean \pm SEM
873 (connecting bars), (n) Representative images of vehicle (left), cerulenin $1\mu\text{g}/\text{mL}$, (right). b-tubulin
874 (cyan), phalloidin (magenta), DAPI (blue). Scale bar= $50\ \mu\text{m}$. Illustrations were done using
875 Biorender®.

876

877 **Figure 3. A high saturated fat diet significantly alters MK phenotype and reduces platelet**
878 **counts.** (a) Schematic of click-chemistry technique where fatty acids modified with an alkyne are
879 supplemented into murine bone marrow HSPC cultures. After 4 days of culture, the fatty acid with
880 the alkyne that incorporated into mature MKs was functionalized with an azide-linked fluorescent
881 reporter to visualize its uptake into cells. (b) Murine bone marrow HSPCs from wildtype mice were
882 incubated with $100\mu\text{M}$ of modified palmitic acid. After 4 days of maturation, MKs were isolated,
883 and the azide-linked fluorescent reported was added. The incorporation of palmitic acid (PA) was
884 visualized using confocal microscopy. PA-alkyne (cyan); DAPI (blue). Scale bar= $5\ \mu\text{m}$. (c) MFI of
885 MKs incubated with 10 and $100\ \mu\text{M}$ PA was calculated using ImageJ. $n=3$, one-way ANOVA –
886 Dunnett's test (d) Murine bone marrow HSPCs from wildtype mice were cultured with TPO and
887 supplemented with 10 and $300\ \mu\text{M}$ palmitic acid. Representative images show MK size. MK area
888 was quantified using ImageJ. $n=4$, one-way ANOVA – Dunnett's test, scale bar= $150\ \mu\text{m}$. (e) To
889 examine proplatelet formation, mature MKs (day 4) were supplemented with palmitic acid (100
890 mM) or DMEM with 0.1% BSA (vehicle), the percentage of MKs making proplatelets at 24h was
891 quantified using the Incucyte high content imaging system. $n=4$, unpaired t-test, two-tailed (f) Male
892 mice were fed a 60% high fat (D12492, Research Diets Inc) or chow diet (D12450B, Research
893 Diets Inc) for 14 weeks. $n=16$, unpaired t-test (g) Mice were weighed at week 14, $n=16$ mice per
894 group, unpaired t-test (h) LT-HSC, ST-HSC, Pre MKs, and MKP cell populations were quantified
895 at week 14 using flow cytometry, $n=4$, unpaired t-test (i) Representative images of bone marrow
896 showing MKs (CD41, blue) and vasculature (laminin, pink) in femur cryosections. Scale bar= 50
897 μm (j) MK area and number were quantified manually from femur cryosections using ImageJ.
898 CHOW $n=4$ and DIO $n=7$, biological replicates, unpaired t-test, (k) Platelet counts were measured
899 using a Sysmex hematology analyzer. CHOW $n=12$ and DIO $n=16$ biological replicates, unpaired
900 t-test, two-tailed. Illustrations were done using Biorender®. All data are presented as mean \pm
901 SD.

902

903 **Figure 4. Platelet counts can be modified in vivo by altering dietary polyunsaturated fatty**
904 **acid composition.** (a) Murine bone marrow HSPCs were incubated with arachidonic acid
905 modified with an alkyne group (3 and $10\ \mu\text{M}$). After 4 days, MKs were isolated and a fluorescently-
906 conjugated azide was added. Incorporation of arachidonic acid was visualized using confocal
907 microscopy and MFI was calculated using ImageJ. $n=3$, one-way ANOVA – Dunnett's test. Yellow:
908 AA-alkyne (yellow), DAPI (blue); Scale bar= $5\ \mu\text{m}$. (b) Murine bone marrow HSPCs from wildtype
909 mice were cultured with TPO and supplemented with arachidonic acid (3 and $10\ \mu\text{M}$). On day 4,
910 MK area was quantified using ImageJ. $n=6$ and $n=3$, respectively, one-way ANOVA – Dunnett's
911 test (c) Mature MKs (day 4) were cultured with arachidonic acid at indicated dosages and the
912 percentage of MKs making proplatelets at 24h was quantified using the Incucyte high content
913 imaging system. $n=3$, unpaired t-test, two-tailed (d) Male mice were fed a 60% high fat diet
914 enriched in polyunsaturated fatty acids (PUFAs) (D22050406i, Research Diets Inc) or chow diet
915 (D12450B, Research Diets Inc) for 12 weeks. $n=10$ mice per group. Body weight (e) and glucose
916 levels (f) were measured, $n=10$, 2-way ANOVA, and unpaired t-test, two-tailed, respectively.
917 Platelet counts were measured at week 4 (g) and 12 (h) using a Sysmex hematology analyzer.
918 $n=10$, unpaired t-test, two-tailed. Newly made platelets were analyzed by quantifying (i)

919 percentage and (j) absolute platelet numbers positive for thiazole orange by flow cytometry,
920 CHOW n=5 and PUFA n=4 biological replicates, unpaired t-test, two-tailed. (k) Representative
921 images showing MKs (CD41, blue) and vasculature (laminin, pink) in femur cryosections at week
922 12. Scale bar=50 μ m (l) MK area and number were quantified from femur cryosections using
923 ImageJ, CHOW n=4 and PUFA n=3 biological replicates, unpaired t-test, two-tailed. (m) Ploidy
924 analysis of native bone marrow MKs assessed by propidium iodide staining and quantified by flow
925 cytometry. n=5, two-way ANOVA. Illustrations were done using Biorender®. All data are
926 presented as mean +/- SD.

927

928 **Figure 5. Lack of CD36 in mice reduces cellular fatty acid incorporation and impairs**
929 **proplatelet formation.** Platelets and MKs were characterized in adult male wildtype (WT) and
930 *Cd36*^{-/-} mice. (a) Platelet counts, mean platelet volume (MPV), and platelet distribution (PDW)
931 were measured using the Sysmex. WT, n=16 and *Cd36*^{-/-}, n=20 biological replicates, unpaired t-
932 test, two-tailed. (b) Red blood cell and monocyte counts were measured using Sysmex, unpaired
933 t-test, two-tailed, WT n=16 and *Cd36*^{-/-} n=20 biological replicates (c-e) HSCs from WT and *Cd36*^{-/-}
934 mice were cultured with palmitic acid or arachidonic acid modified with an alkyne group at
935 indicated dosages. After 4 days of maturation, MKs were isolated, and click-chemistry performed
936 as described. (c) Representative images of MKs from WT and *Cd36*^{-/-} mice. MFI was calculated
937 using ImageJ. Blue: palmitic acid (100 μ M). scale bar=5 μ m. Incorporation of palmitic acid (d)
938 and (e) arachidonic acid were visualized using confocal microscopy and MFI was calculated using
939 ImageJ. WT n=3 and *Cd36*^{-/-} n=4 biological replicates, unpaired t-test, two-tailed (f) Murine bone
940 marrow HSPCs from WT and *Cd36*^{-/-} mice were cultured with TPO. After 4 days of maturation,
941 the number of mature MKs (CD41/CD42d+ cells) was measured using flow cytometry, WT n=3
942 and *Cd36*^{-/-} n=4 biological replicates, unpaired t-test, two-tailed. (g) MK number and area were
943 quantified from femur cryosections using ImageJ. WT n=3 and *Cd36*^{-/-} n=4 biological replicates,
944 unpaired t-test. Representative images show MKs (CD41, blue) and vasculature (laminin, pink).
945 Scale bar=50 μ m (h) Ploidy analysis of cultured bone marrow MKs assessed by propidium iodide
946 staining and flow cytometry. Percentage of CD41+ cells with different levels of ploidy is shown.
947 n=4, two-way ANOVA. (i-j) Proplatelet formation was quantified from mature MKs (day 4) from
948 WT and *Cd36*^{-/-} mice in the presence of hirudin. (i) Representative graph of proplatelet area from
949 n=4. Data are presented as mean +/- SEM (connecting bars) (j) and proplatelet percentage at 24h,
950 were quantified using the Incucyte high content imaging system. n= 6, unpaired t-test, two-tailed.
951 All data are presented as mean +/- SD.

952

953 **Figure 6. Megakaryocytes and platelet counts in *Cd36*^{-/-} mice are not affected by high fat**
954 **diets enriched in fatty acids.** Adult male WT and *Cd36*^{-/-} mice were fed chow or high fat diets
955 enriched in saturated or polyunsaturated fatty acids as in Figures 3 and 4, respectively, for 13
956 weeks. (a-b) At week 8, (a) platelet counts and (b) mean platelet volume (MPV) were measured
957 using Sysmex hematology analyzer and (c) newly made platelets were analyzed by quantifying
958 percentage and absolute platelet numbers positive for thiazole orange by flow cytometry. n=3
959 (CHOW), n=4 (DIO) and n=3 (PUFA) mice per group, One-way Anova test, Dunnett's multiple
960 comparisons test. At week 13, (d) platelet counts, (e) MPV and (f) newly made platelets were
961 measured as above. (g) Representative images showing MKs (CD41, blue) and vasculature
962 (laminin, pink) in femur cryosections at week 13 in indicated treatment groups. Scale bar=50 μ m.
963 (h) MK area and (i) number were quantified from femur cryosections using ImageJ, n=3 mice per
964 group. One-way Anova test, Dunnett's multiple comparisons test. All data are presented as mean
965 +/- SD.

966

967 **Figure 7. Identification of a CD36 loss-of-function variant (p.Tyr325Ter) in patients with**
968 **thrombocytopenia.** (a) Family pedigree including affected mother (I:2) and patients II.1 and II.2.
969 highlighted in solid black. Asterisks (*) indicate patients whose whole exomes were sequenced.
970 (b) Patient's details and hematological parameters. Hematological parameters of patients II.1 and
971 II.2. MPV values are shown in the table as 'Large' because platelets with large volume are
972 undetectable by Sysmex analyzer. (c) The nonsense variant c.975T>G; p. Tyr325Ter results in
973 the substitution of tyrosine residue at position 325 to a stop codon which is predicted to truncate
974 the full length of 472 amino acids. (d) Mutation details (e) Western blot of protein lysate from
975 patient platelets showing truncation of CD36 protein and GAPDH loading control (f) Conservation
976 of tyrosine 325 residue across multiple species. The location of the tyrosine residue is shown by
977 the highlighted green box. (g) Modelled structure of the CD36 ectodomain using homology
978 modeling.²² The structure shows the result of the CD36 nonsense variant on the structure of the
979 WT CD36 protein (left) and mutant CD36 (right) because of the truncation. (h) Schematic of the
980 CD36 protein structure. CD36 has two short cytoplasmic domains representing the C-terminal
981 and N-terminals, two transmembrane domains and two large extracellular domains. The
982 extracellular domain contains three disulfide bonds, binding sites of interaction with
983 thrombospondin type I repeat (TSR), plasmodium falciparum, oxLDL, sites of acetylation
984 (palmitoylation), phosphorylation, glycosylation, and the position of the nonsense variant found in
985 patients II.1 and II.2.^{56,57} (i) Protein expression of transfected CD36-wild type and CD36 mutants.
986 C: pEF6 empty vector; WT: pEF6/CD36 wild type; Del: pEF6/CD36 deleted mutant; Sub:
987 pEF6/CD36 substitution mutant. SDS-PAGE immunoblot expression analysis of samples probed
988 with anti-CD36 and anti-GAPDH antibodies. Expected sizes of the samples are indicated on the
989 right. (j) NFAT-luciferase activity measuring activation of CD36 after normalization of the
990 stimulated and unstimulated conditions. Only WT CD36 shows luciferase activity over
991 background. n=3 biological replicates, One-way Anova test with Dunnett's test. Data are
992 presented as mean +/- SD.

993 *M: male, F: female, WBC: white blood cell, RBC: red blood cell, Mono: monocyte, IPF: immature*
994 *platelet fraction, MPV: mean platelet volume. WT: wildtype, Del: deletion, Sub: substitution*

995

996 **REFERENCES**

- 997 1 van Meer, G., Voelker, D. R. & Feigenson, G. W. Membrane lipids: where they are and
 998 how they behave. *Nat Rev Mol Cell Biol* **9**, 112-124, doi:10.1038/nrm2330 (2008).
- 999 2 Murphy, A. J. *et al.* ApoE regulates hematopoietic stem cell proliferation, monocytosis,
 1000 and monocyte accumulation in atherosclerotic lesions in mice. *J Clin Invest* **121**, 4138-
 1001 4149, doi:10.1172/JCI57559 (2011).
- 1002 3 Bansal, P. *et al.* Current Updates on Role of Lipids in Hematopoiesis. *Infect Disord Drug*
 1003 *Targets* **18**, 192-198, doi:10.2174/1871526518666180405155015 (2018).
- 1004 4 Lee, M. K. S., Al-Sharea, A., Dragoljevic, D. & Murphy, A. J. Hand of FATE: lipid
 1005 metabolism in hematopoietic stem cells. *Curr Opin Lipidol* **29**, 240-245,
 1006 doi:10.1097/MOL.0000000000000500 (2018).
- 1007 5 Pernes, G., Flynn, M. C., Lancaster, G. I. & Murphy, A. J. Fat for fuel: lipid metabolism in
 1008 haematopoiesis. *Clin Transl Immunology* **8**, e1098, doi:10.1002/cti2.1098 (2019).
- 1009 6 Collins, J. M. *et al.* De novo lipogenesis in the differentiating human adipocyte can
 1010 provide all fatty acids necessary for maturation. *J Lipid Res* **52**, 1683-1692,
 1011 doi:10.1194/jlr.M012195 (2011).
- 1012 7 Noetzli, L. J., French, S. L. & Machlus, K. R. New Insights Into the Differentiation of
 1013 Megakaryocytes From Hematopoietic Progenitors. *Arterioscler Thromb Vasc Biol* **39**,
 1014 1288-1300, doi:10.1161/ATVBAHA.119.312129 (2019).
- 1015 8 Machlus, K. R. & Italiano, J. E. The incredible journey: From megakaryocyte
 1016 development to platelet formation. *J Cell Biol* **201**, 785-796, doi:10.1083/jcb.201304054
 1017 (2013).
- 1018 9 Pietras, E. M. *et al.* Functionally Distinct Subsets of Lineage-Biased Multipotent
 1019 Progenitors Control Blood Production in Normal and Regenerative Conditions. *Cell stem*
 1020 *cell* **17**, 35-46, doi:10.1016/j.stem.2015.05.003 (2015).
- 1021 10 Eckly, A. *et al.* Biogenesis of the demarcation membrane system (DMS) in
 1022 megakaryocytes. *Blood* **123**, 921-930, doi:10.1182/blood-2013-03-492330 (2014).
- 1023 11 Whitaker, B., Rajbhandary, S., Kleinman, S., Harris, A. & Kamani, N. Trends in United
 1024 States blood collection and transfusion: results from the 2013 AABB Blood Collection,
 1025 Utilization, and Patient Blood Management Survey. *Transfusion* **56**, 2173-2183,
 1026 doi:10.1111/trf.13676 (2016).
- 1027 12 Provan, D. *et al.* Updated international consensus report on the investigation and
 1028 management of primary immune thrombocytopenia. *Blood Adv* **3**, 3780-3817,
 1029 doi:10.1182/bloodadvances.2019000812 (2019).
- 1030 13 Ghanima, W. *et al.* Bone marrow fibrosis in 66 patients with immune thrombocytopenia
 1031 treated with thrombopoietin-receptor agonists: a single-center, long-term follow-up.
 1032 *Haematologica* **99**, 937-944, doi:10.3324/haematol.2013.098921 (2014).
- 1033 14 Mitchell, W. B. & Bussel, J. B. Thrombopoietin receptor agonists: a critical review. *Semin*
 1034 *Hematol* **52**, 46-52, doi:10.1053/j.seminhematol.2014.11.001 (2015).
- 1035 15 Prica, A., Sholzberg, M. & Buckstein, R. Safety and efficacy of thrombopoietin-receptor
 1036 agonists in myelodysplastic syndromes: a systematic review and meta-analysis of
 1037 randomized controlled trials. *Br J Haematol* **167**, 626-638, doi:10.1111/bjh.13088 (2014).

1038 16 Manni, M. M. *et al.* Acyl chain asymmetry and polyunsaturation of brain phospholipids
1039 facilitate membrane vesiculation without leakage. *Elife* **7**, doi:10.7554/eLife.34394
1040 (2018).

1041 17 Valet, C. *et al.* Adipocyte Fatty Acid Transfer Supports Megakaryocyte Maturation. *Cell*
1042 *Rep* **32**, 107875, doi:10.1016/j.celrep.2020.107875 (2020).

1043 18 Kelly, K. L. *et al.* De novo lipogenesis is essential for platelet production in humans. *Nat*
1044 *Metab* **2**, 1163-1178, doi:10.1038/s42255-020-00272-9 (2020).

1045 19 Machlus, K. R. *et al.* Synthesis and dephosphorylation of MARCKS in the late stages of
1046 megakaryocyte maturation drive proplatelet formation. *Blood* **127**, 1468-1480,
1047 doi:10.1182/blood-2015-08-663146 (2016).

1048 20 Febbraio, M. *et al.* A null mutation in murine CD36 reveals an important role in fatty acid
1049 and lipoprotein metabolism. *J Biol Chem* **274**, 19055-19062,
1050 doi:10.1074/jbc.274.27.19055 (1999).

1051 21 Aitman, T. J. *et al.* Malaria susceptibility and CD36 mutation. *Nature* **405**, 1015-1016,
1052 doi:10.1038/35016636 (2000).

1053 22 Hsieh, F. L. *et al.* The structural basis for CD36 binding by the malaria parasite. *Nat*
1054 *Commun* **7**, 12837, doi:10.1038/ncomms12837 (2016).

1055 23 Escribá, P. V. *et al.* Membrane lipid therapy: Modulation of the cell membrane
1056 composition and structure as a molecular base for drug discovery and new disease
1057 treatment. *Prog Lipid Res* **59**, 38-53, doi:10.1016/j.plipres.2015.04.003 (2015).

1058 24 Doi, O., Doi, F., Schroeder, F., Alberts, A. W. & Vagelos, P. R. Manipulation of fatty acid
1059 composition of membrane phospholipid and its effects on cell growth in mouse LM cells.
1060 *Biochim Biophys Acta* **509**, 239-250, doi:10.1016/0005-2736(78)90044-5 (1978).

1061 25 Pinot, M. *et al.* Lipid cell biology. Polyunsaturated phospholipids facilitate membrane
1062 deformation and fission by endocytic proteins. *Science* **345**, 693-697,
1063 doi:10.1126/science.1255288 (2014).

1064 26 Hales, C. M., Carroll, M. D., Fryar, C. D. & Ogden, C. L. Prevalence of Obesity and
1065 Severe Obesity Among Adults: United States, 2017-2018. *NCHS Data Brief*, 1-8 (2020).

1066 27 Yin, R., Wang, X., Li, K., Yu, K. & Yang, L. Lipidomic profiling reveals distinct differences
1067 in plasma lipid composition in overweight or obese adolescent students. *BMC Endocr*
1068 *Disord* **21**, 201, doi:10.1186/s12902-021-00859-7 (2021).

1069 28 Vilahur, G., Ben-Aicha, S. & Badimon, L. New insights into the role of adipose tissue in
1070 thrombosis. *Cardiovasc Res* **113**, 1046-1054, doi:10.1093/cvr/cvx086 (2017).

1071 29 Badimon, L., Hernández Vera, R., Padró, T. & Vilahur, G. Antithrombotic therapy in
1072 obesity. *Thromb Haemost* **110**, 681-688, doi:10.1160/th12-12-0928 (2013).

1073 30 Barale, C. & Russo, I. Influence of Cardiometabolic Risk Factors on Platelet Function. *Int*
1074 *J Mol Sci* **21**, doi:10.3390/ijms21020623 (2020).

1075 31 Haas, S. *et al.* Inflammation-Induced Emergency Megakaryopoiesis Driven by
1076 Hematopoietic Stem Cell-like Megakaryocyte Progenitors. *Cell Stem Cell* **17**, 422-434,
1077 doi:10.1016/j.stem.2015.07.007 (2015).

1078 32 Couldwell, G. & Machlus, K. R. Modulation of megakaryopoiesis and platelet production
1079 during inflammation. *Thromb Res* **179**, 114-120, doi:10.1016/j.thromres.2019.05.008
1080 (2019).

1081 33 Blüher, M. Metabolically Healthy Obesity. *Endocrine Reviews* **41**,
1082 doi:10.1210/edrv/bnaa004 (2020).

1083 34 Iacobini, C., Pugliese, G., Blasetti Fantauzzi, C., Federici, M. & Menini, S. Metabolically
1084 healthy versus metabolically unhealthy obesity. *Metabolism* **92**, 51-60,
1085 doi:10.1016/j.metabol.2018.11.009 (2019).

1086 35 Xu, S., Jay, A., Brunaldi, K., Huang, N. & Hamilton, J. A. CD36 enhances fatty acid
1087 uptake by increasing the rate of intracellular esterification but not transport across the
1088 plasma membrane. *Biochemistry* **52**, 7254-7261, doi:10.1021/bi400914c (2013).

1089 36 Podrez, E. A. *et al.* Platelet CD36 links hyperlipidemia, oxidant stress and a
1090 prothrombotic phenotype. *Nat Med* **13**, 1086-1095, doi:10.1038/nm1626 (2007).

1091 37 Meng, O. *et al.* Loss of Cd36 Expression Has Limited Impact on Mouse Normal
1092 Hematopoiesis. *Blood* **140**, 11395-11396, doi:10.1182/blood-2022-171125 (2022).

1093 38 Xu, X., Zheng, X. & Zhu, F. CD36 gene variants and their clinical relevance: a narrative
1094 review. *Annals of Blood* **6** (2021).

1095 39 Tomiyama, Y. *et al.* Identification of the platelet-specific alloantigen, Naka, on platelet
1096 membrane glycoprotein IV. *Blood* **75**, 684-687 (1990).

1097 40 Strassheim, D. *et al.* Metabolite G-Protein Coupled Receptors in Cardio-Metabolic
1098 Diseases. *Cells* **10**, doi:10.3390/cells10123347 (2021).

1099 41 Vijey, P., Posorske, B. & Machlus, K. R. In vitro culture of murine megakaryocytes from
1100 fetal liver-derived hematopoietic stem cells. *Platelets* **29**, 583-588,
1101 doi:10.1080/09537104.2018.1492107 (2018).

1102 42 Heib, T., Gross, C., Muller, M. L., Stegner, D. & Pleines, I. Isolation of murine bone
1103 marrow by centrifugation or flushing for the analysis of hematopoietic cells - a
1104 comparative study. *Platelets* **32**, 601-607, doi:10.1080/09537104.2020.1797323 (2021).

1105 43 Strassel, C. *et al.* Hirudin and heparin enable efficient megakaryocyte differentiation of
1106 mouse bone marrow progenitors. *Exp Cell Res* **318**, 25-32,
1107 doi:10.1016/j.yexcr.2011.10.003 (2012).

1108 44 Huynh, K. *et al.* Lipidomic Profiling of Murine Macrophages Treated with Fatty Acids of
1109 Varying Chain Length and Saturation Status. *Metabolites* **8**,
1110 doi:10.3390/metabo8020029 (2018).

1111 45 Weir, J. M. *et al.* Plasma lipid profiling in a large population-based cohort. *J Lipid Res* **54**,
1112 2898-2908, doi:10.1194/jlr.P035808 (2013).

1113 46 Huynh, K. *et al.* High-Throughput Plasma Lipidomics: Detailed Mapping of the
1114 Associations with Cardiometabolic Risk Factors. *Cell Chem Biol* **26**, 71-84.e74,
1115 doi:10.1016/j.chembiol.2018.10.008 (2019).

1116 47 Liebisch, G. *et al.* Update on LIPID MAPS classification, nomenclature, and shorthand
1117 notation for MS-derived lipid structures. *J Lipid Res* **61**, 1539-1555,
1118 doi:10.1194/jlr.S120001025 (2020).

1119 48 Gillespie, M. *et al.* The reactome pathway knowledgebase 2022. *Nucleic Acids Research*
1120 **50**, D687-D692, doi:10.1093/nar/gkab1028 (2021).

1121 49 French, S. L. *et al.* High-content, label-free analysis of proplatelet production from
1122 megakaryocytes. *J Thromb Haemost* **18**, 2701-2711, doi:10.1111/jth.15012 (2020).

1123 50 Lutz, J. F. & Zarafshani, Z. Efficient construction of therapeutics, bioconjugates,
1124 biomaterials and bioactive surfaces using azide-alkyne "click" chemistry. *Adv Drug Deliv*
1125 *Rev* **60**, 958-970, doi:10.1016/j.addr.2008.02.004 (2008).

1126 51 Hein, C. D., Liu, X. M. & Wang, D. Click chemistry, a powerful tool for pharmaceutical
1127 sciences. *Pharm Res* **25**, 2216-2230, doi:10.1007/s11095-008-9616-1 (2008).

1128 52 Kawamoto, T. Use of a new adhesive film for the preparation of multi-purpose fresh-
1129 frozen sections from hard tissues, whole-animals, insects and plants. *Arch Histol Cytol*
1130 **66**, 123-143, doi:10.1679/aohc.66.123 (2003).

1131 53 Watson, S. P., Lowe, G. C., Lordkipanidzé, M. & Morgan, N. V. Genotyping and
1132 phenotyping of platelet function disorders. *J Thromb Haemost* **11 Suppl 1**, 351-363,
1133 doi:10.1111/jth.12199 (2013).

1134 54 Johnson, B. *et al.* Whole exome sequencing identifies genetic variants in inherited
1135 thrombocytopenia with secondary qualitative function defects. *Haematologica* **101**, 1170-
1136 1179, doi:10.3324/haematol.2016.146316 (2016).

1137 55 Thorne, R. F. *et al.* The Integrins $\alpha 3\beta 1$ and $\alpha 6\beta 1$ Physically and Functionally Associate
1138 with CD36 in Human Melanoma Cells REQUIREMENT FOR THE EXTRACELLULAR
1139 DOMAIN OF CD36. *Journal of Biological Chemistry* **275**, 35264-35275 (2000).

1140 56 Tomlinson, M. *et al.* Collagen promotes sustained glycoprotein VI signaling in platelets
1141 and cell lines. *Journal of Thrombosis and Haemostasis* **5**, 2274-2283 (2007).

1142 57 Pekelharing, J. *et al.* Haematology reference intervals for established and novel
1143 parameters in healthy adults. *Sysmex Journal International* **20**, 1-9 (2010).

1144

Figure 1

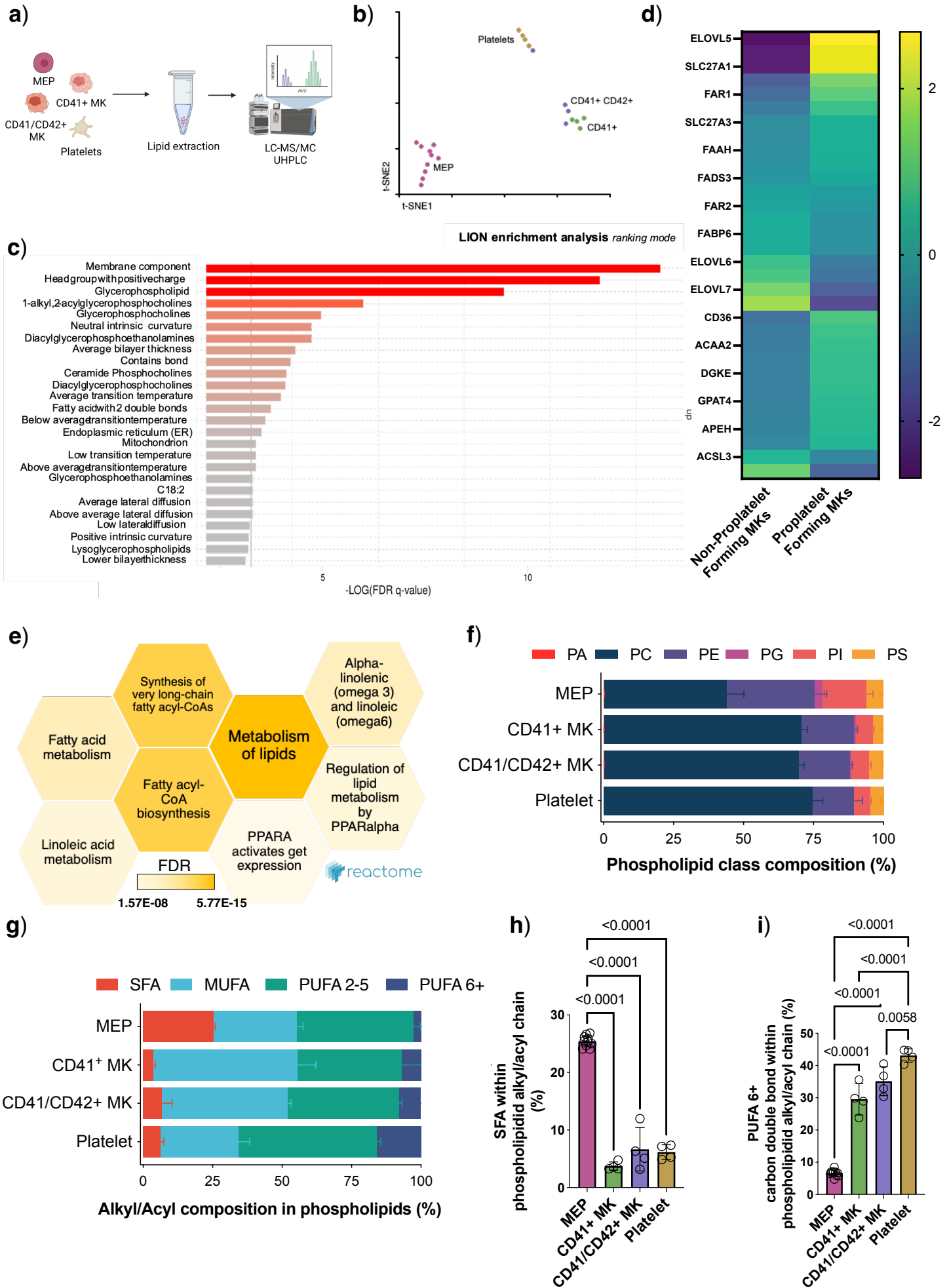


Figure 2

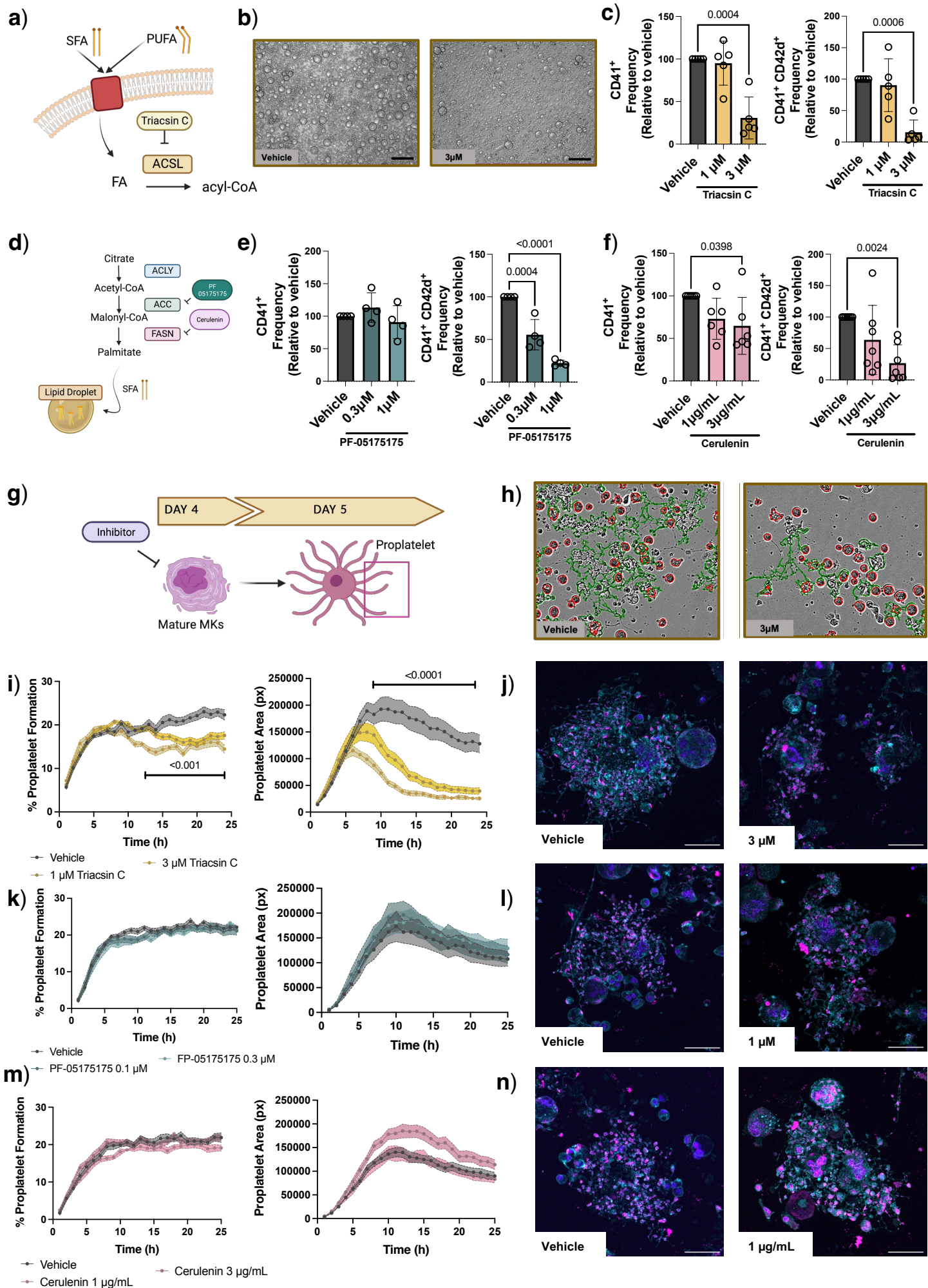


Figure 3

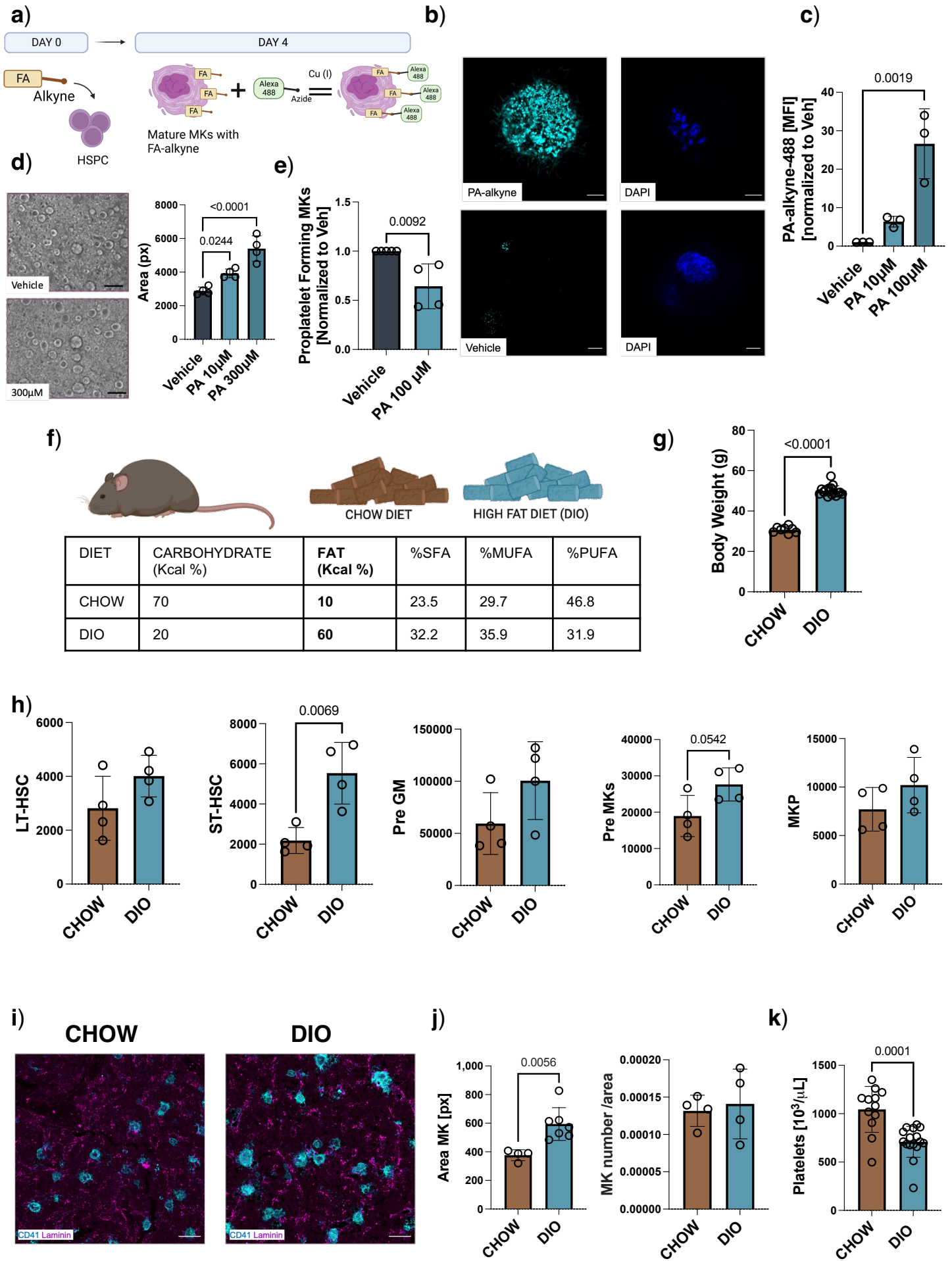


Figure 4

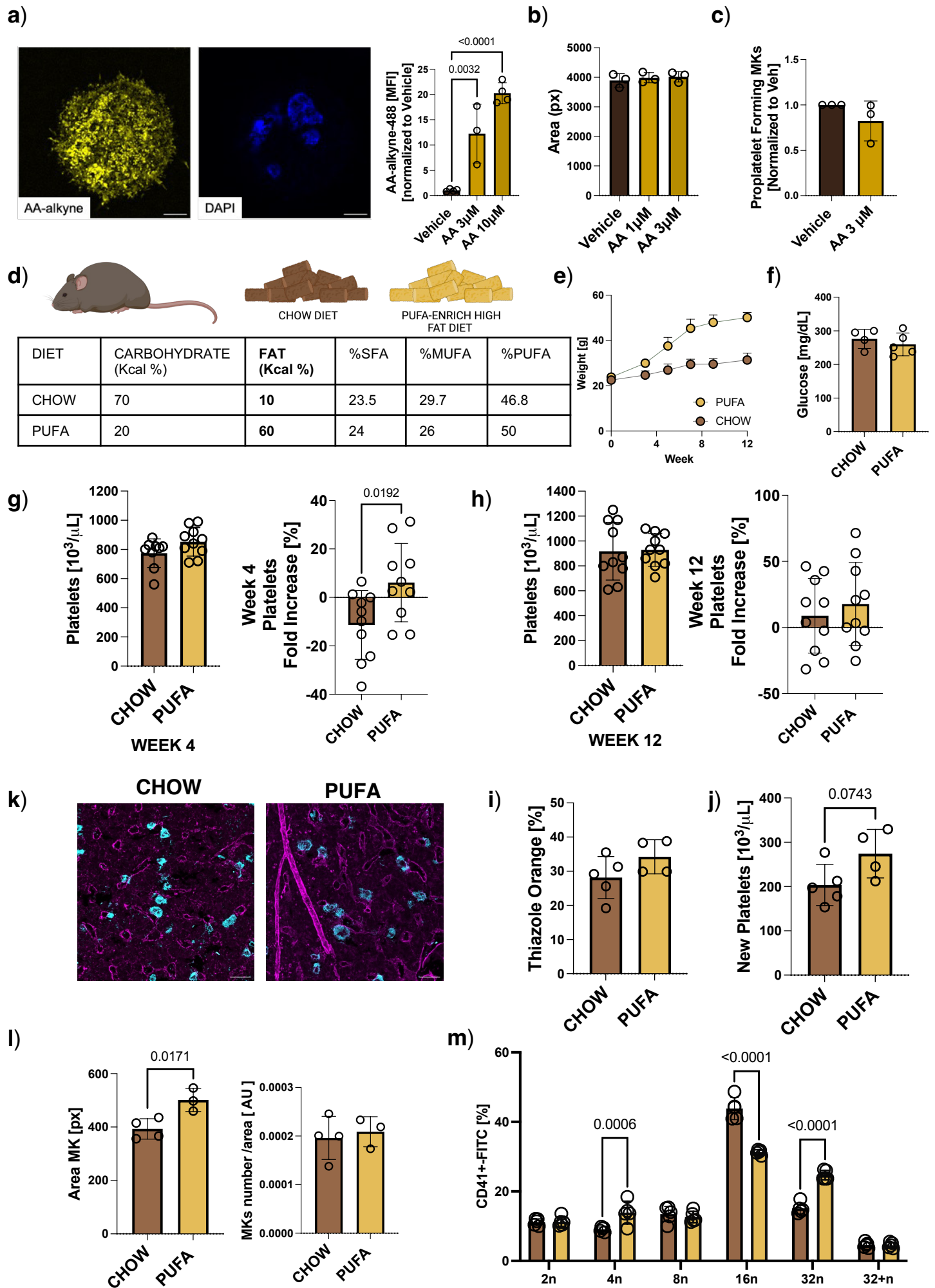


Figure 5

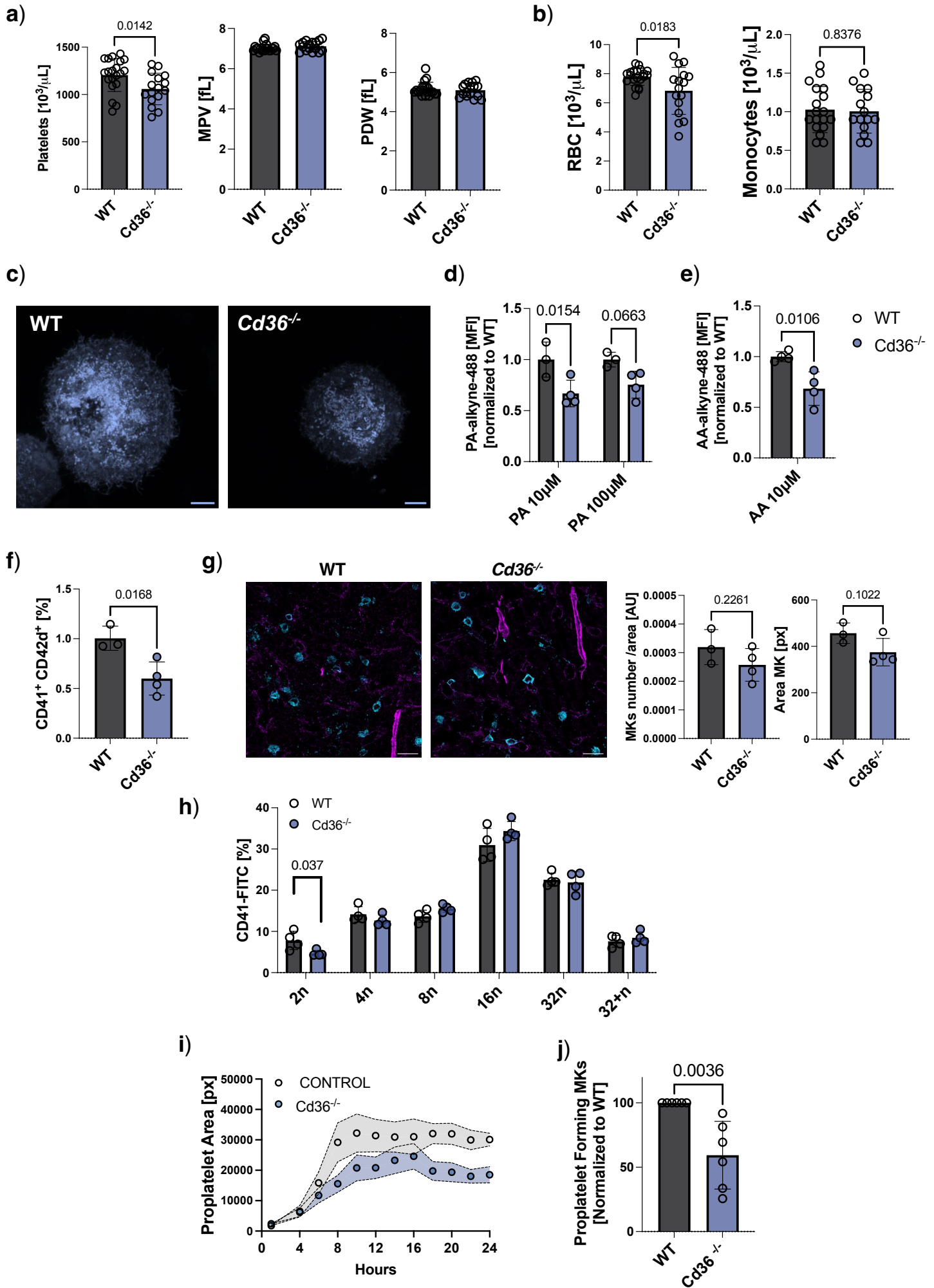


Figure 6

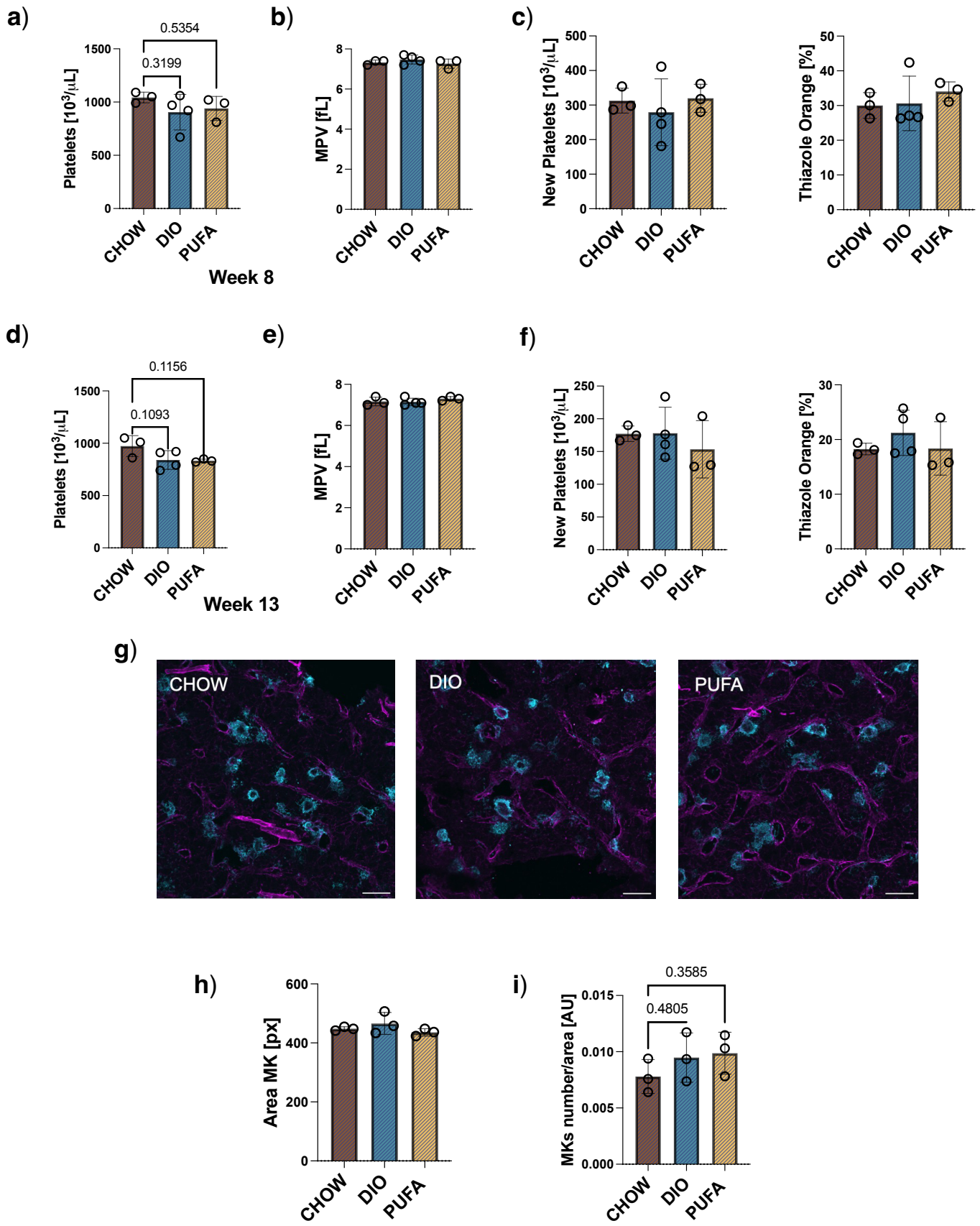
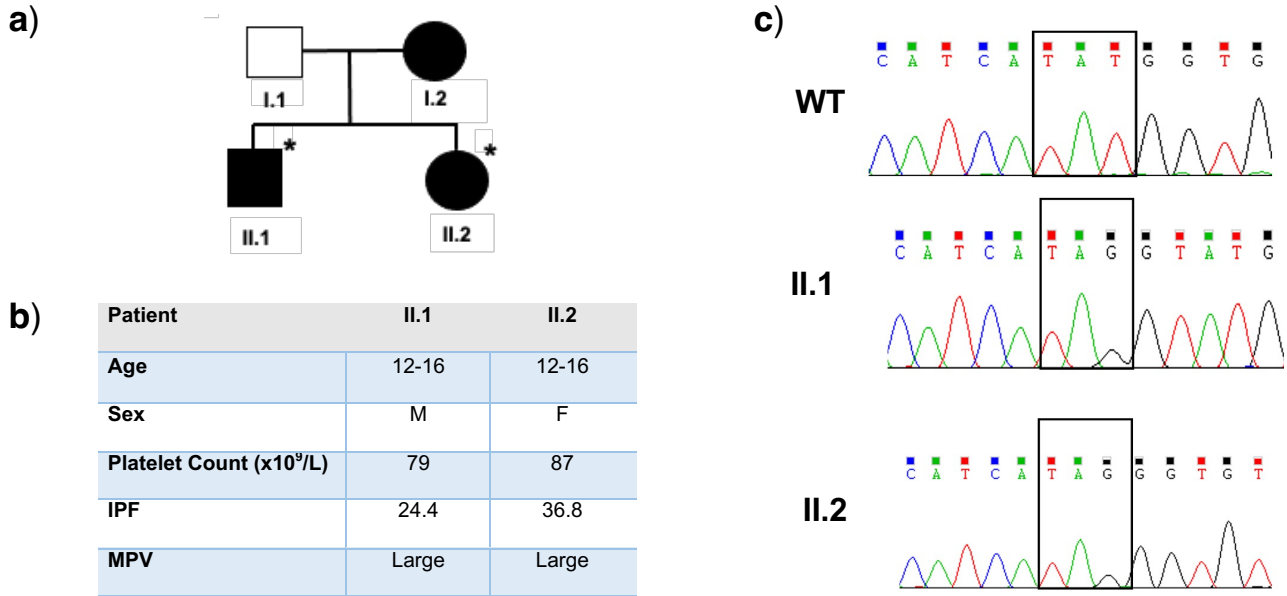
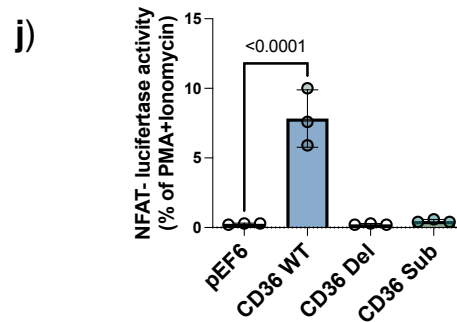
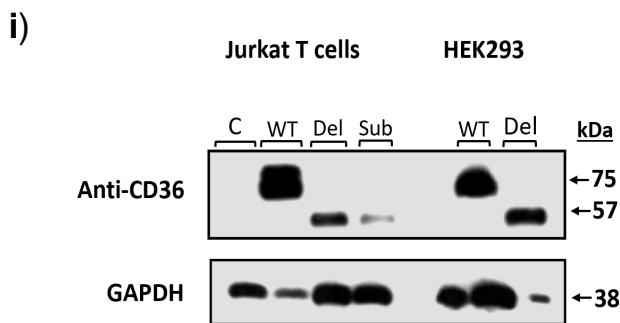
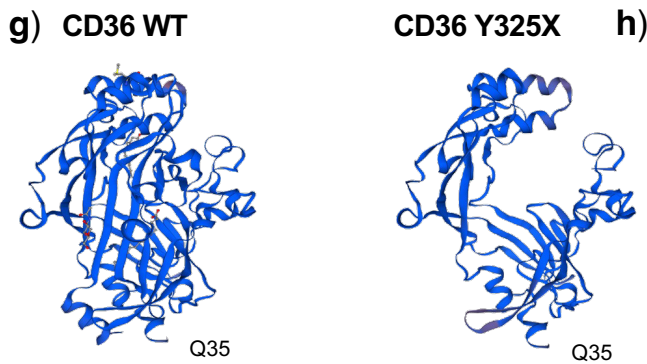
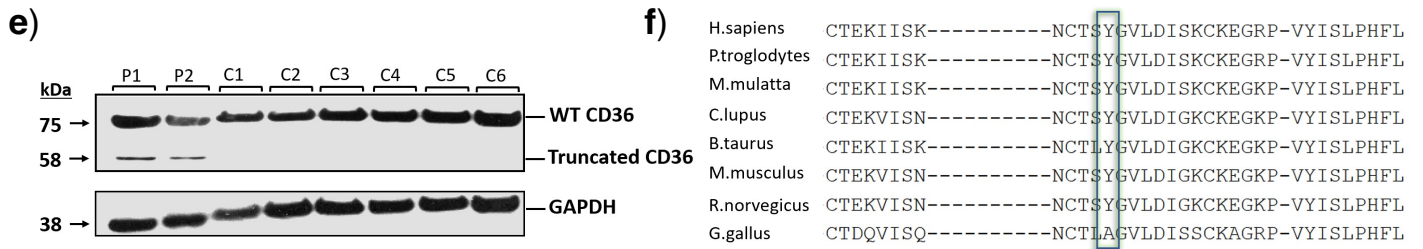


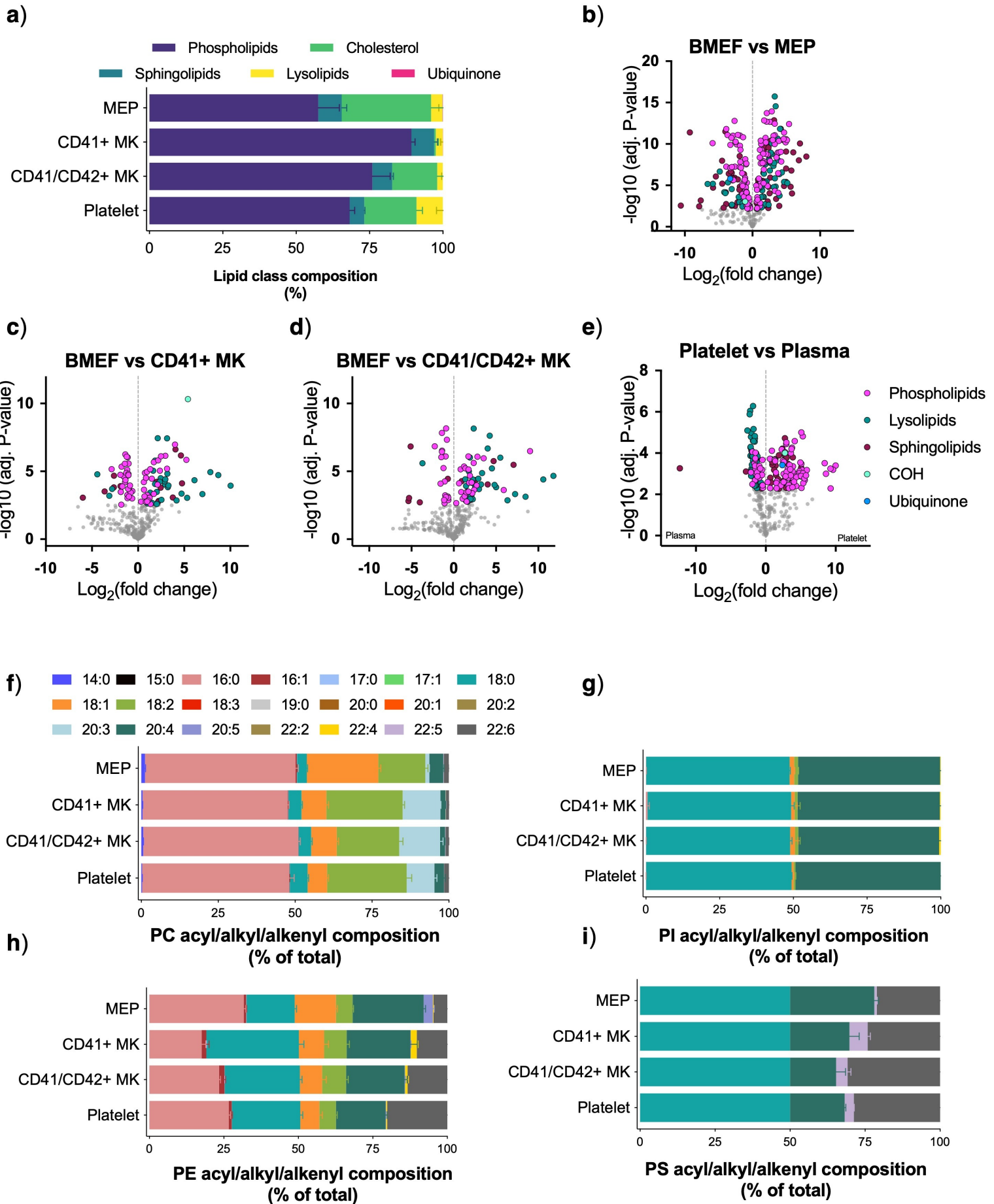
Figure 7



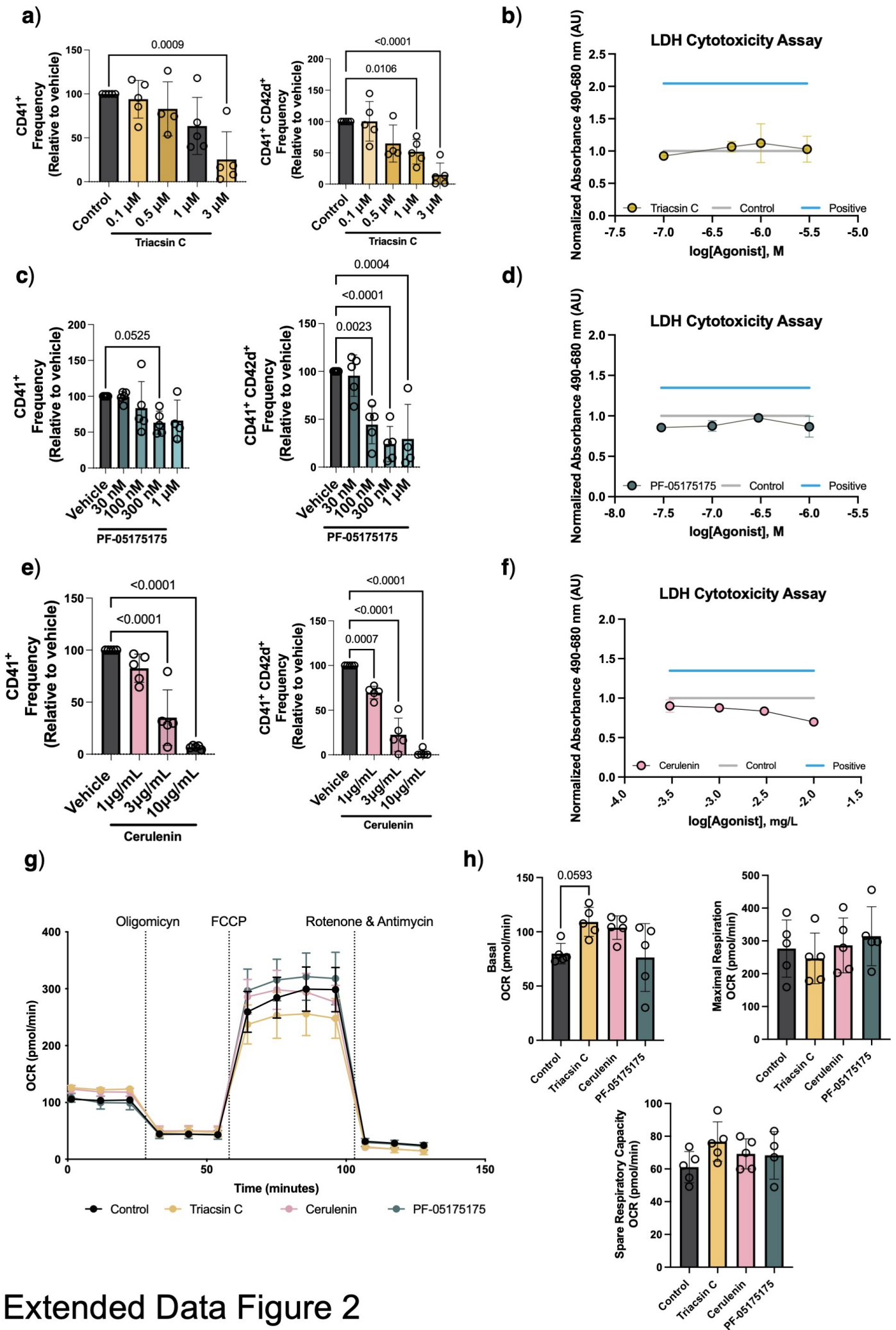
d)

Patient	Gene	Genomic variation	Protein effect	Variation type	Prevalence	Mutation taster	ACMG criteria	Classification
II.1	<i>CD36</i>	c.975T>G	p. Tyr325Ter	stop gained	0.007914	Polymorphism	PVS1,P S3,PP1, PP5	Pathogenic
II.2	<i>CD36</i>	c.975T>G	p. Tyr325Ter	stop gained	0.007914	Polymorphism	PVS1,P S3,PP1, PP5	Pathogenic

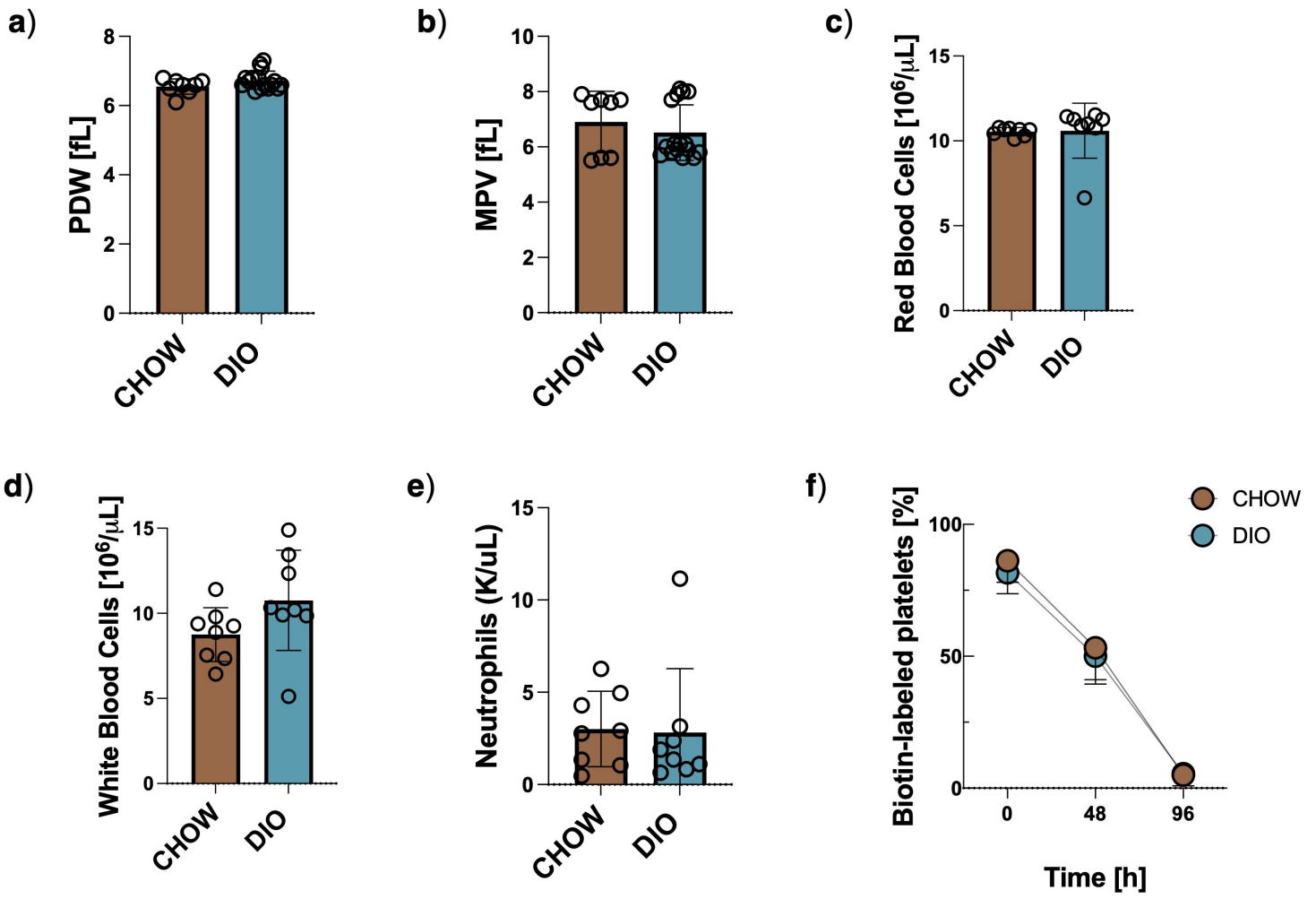




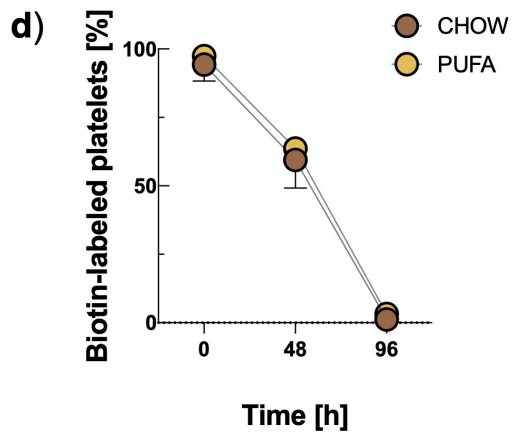
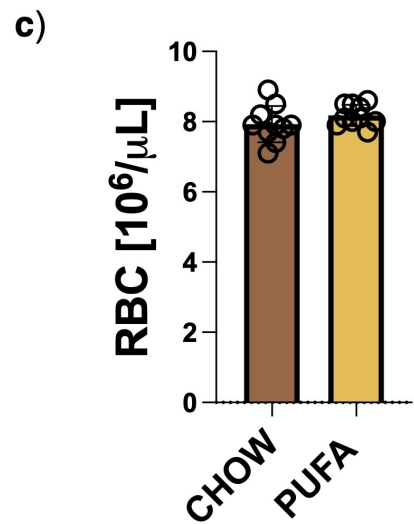
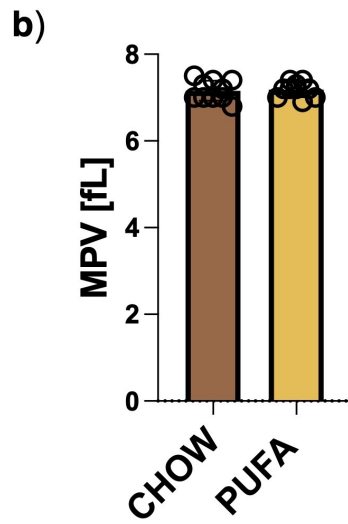
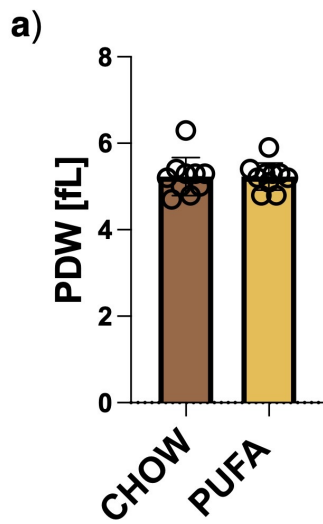
Extended Data Figure 1

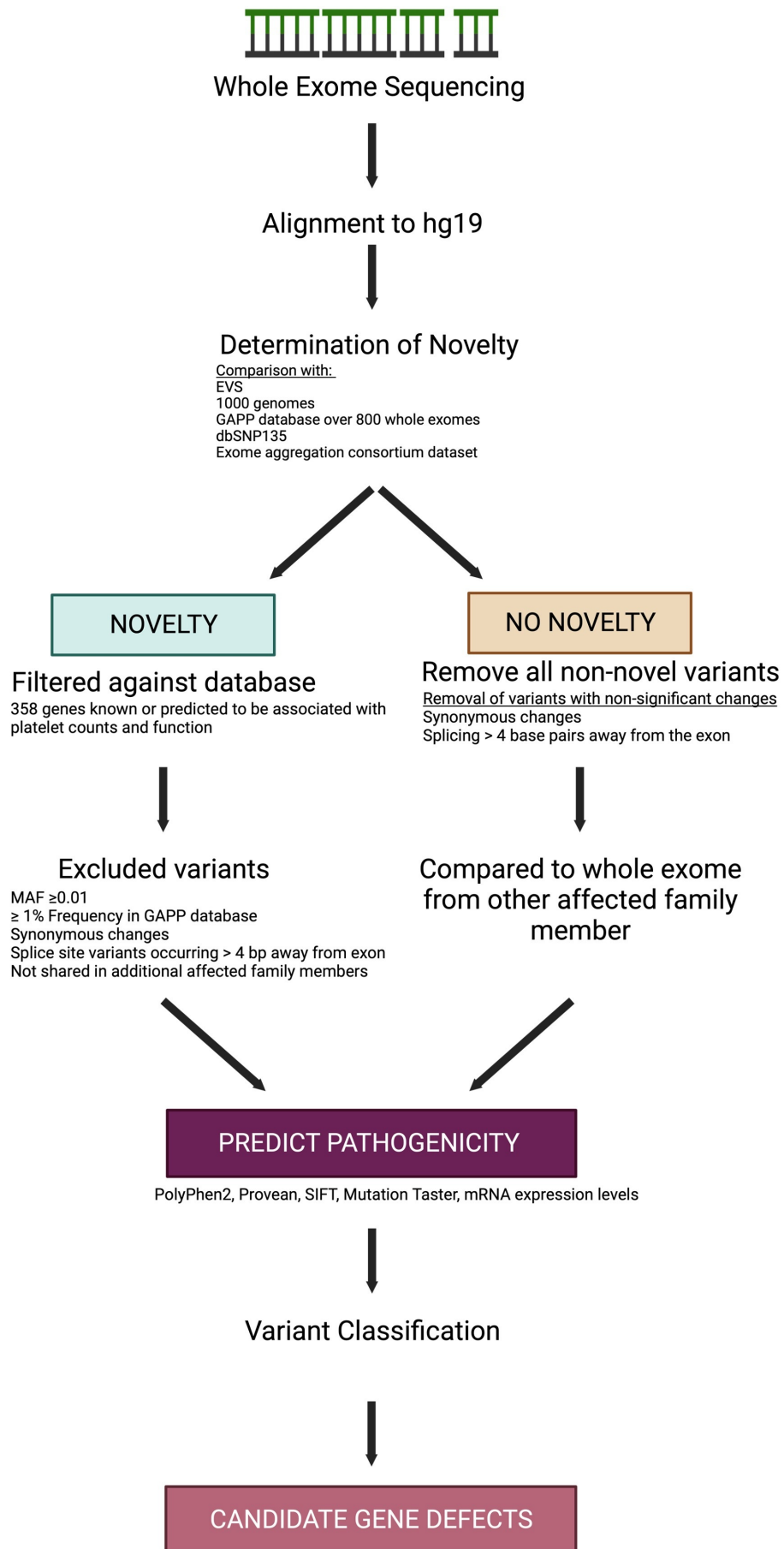


Extended Data Figure 2



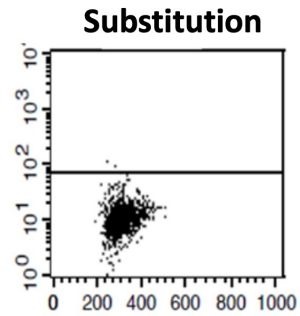
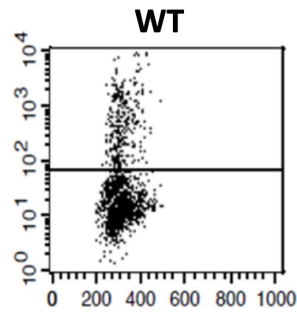
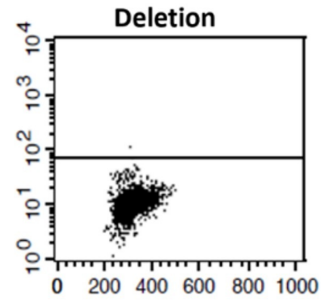
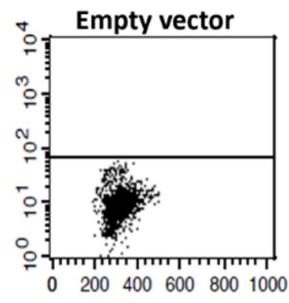
Extended Data Figure 3



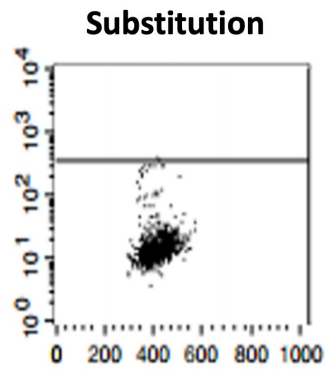
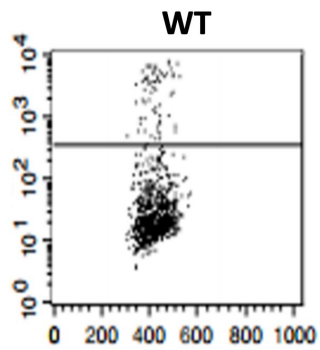
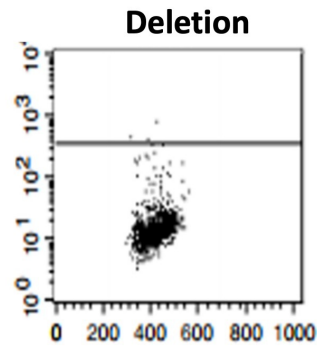
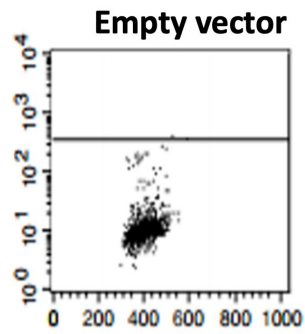


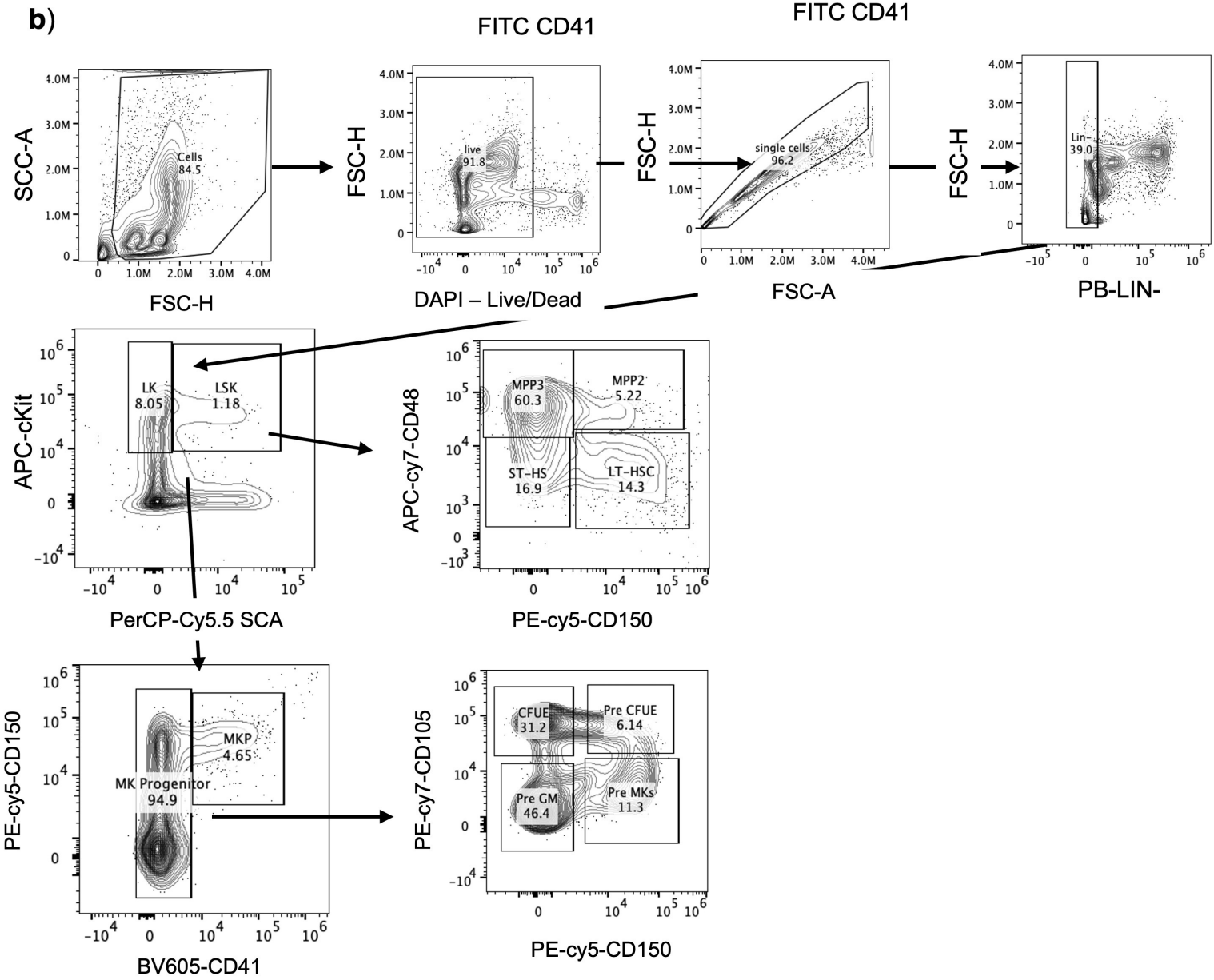
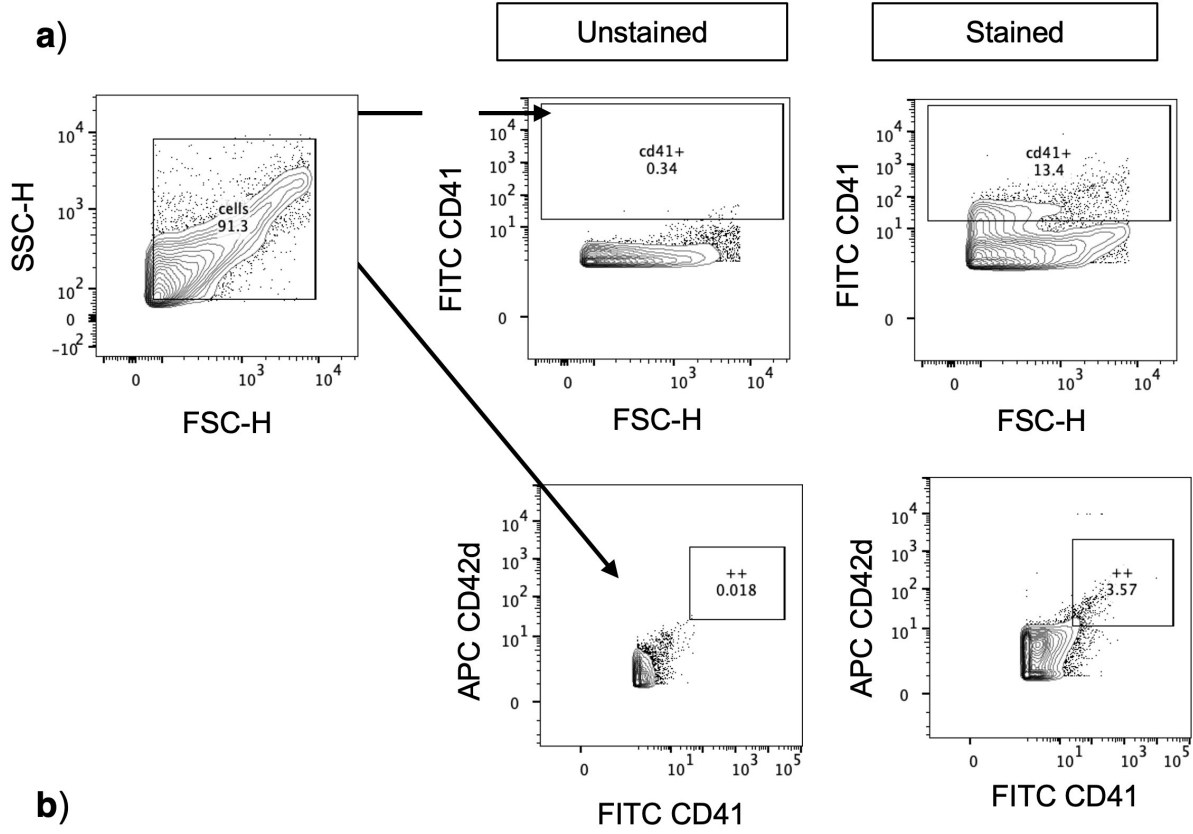
Extended Data Figure 5

a)



b)





Extended Data Figure 7

Extended Data Table 1. Thrombopoietin measurements in plasma from mice fed with chow, DIO and PUFA-enriched diets

	Normal Range	CHOW	DIO	PUFA
Number of values		4	5	5
Mean TPO [pg/mL]	724-3706	838.4	1007	1416
Std. Deviation		93.82	205.4	190.9

Extended Data Table 2: Summary of variants included in UK-GAPP study.

Patients	5.I	5.II
Total number of variants identified by WES	43,774	43,995
Total number of variants within 358 platelet genes panel	233	243
Total number of variants (excluding synonymous and intronic variants)	149	135
Total number of variants with MAF \leq 0.01	26	24
Total number of variants after pathogenicity prediction	19	17
Total shared variants	11	11
Plausible candidate variants	1	1